

Article

Structural Response Prediction of Floating Offshore Wind Turbines Based on Force-to-Motion Transfer Functions and State-Space Models

Jie Xu ¹, Changjie Li ¹, Wei Jiang ², Fei Lin ², Shi Liu ³, Hongchao Lu ^{4,5,*} and Hongbo Wang ^{5,*}

¹ Guangdong Datang International Chaozhou Power Generation Co., Ltd., Chaozhou 515700, China; dtczdc@163.com (J.X.); xuj2887@126.com (C.L.)

² China Datang Co., Ltd. Guangdong Branch, Guangzhou 510000, China; jiangwei_cdt@126.com (W.J.); 13827377631@163.com (F.L.)

³ China Southern Power Grid Electric Power Technology Co., Ltd., Guangzhou 510020, China; 13925041516@139.com

⁴ College of Marine Science and Technology, China University of Geosciences, Wuhan 430074, China

⁵ School of Civil Engineering & Transportation, South China University of Technology, Guangzhou 510641, China

* Correspondence: luhongchao@cug.edu.cn (H.L.); wanghongbo_ic@163.com (H.W.)

Abstract: This paper proposes an innovative algorithm for forecasting the motion response of floating offshore wind turbines by employing force-to-motion transfer functions and state-space models. Traditional numerical integration techniques, such as the Newmark- β method, frequently struggle with inefficiencies due to the heavy computational demands of convolution integrals in the Cummins equation. Our new method tackles these challenges by converting the problem into a system output calculation, thereby eliminating convolutions and potentially enhancing computational efficiency. The procedure begins with the estimation of force-to-motion transfer functions derived from the hydrostatic and hydrodynamic characteristics of the wind turbine. These transfer functions are then utilized to construct state-space models, which compactly represent the system dynamics. Motion responses resulting from initial conditions and wave forces are calculated using these state-space models, leveraging their poles and residues. We validated the proposed method by comparing its calculated responses to those obtained via the Newmark- β method. Initial tests on a single-degree-of-freedom (SDOF) system demonstrated that our algorithm accurately predicts motion responses. Further validation involved a numerical model of a spar-type floating offshore wind turbine, showing high accuracy in predicting responses to both regular and irregular wave conditions, closely aligning with results from conventional methods. Additionally, we assessed the efficiency of our algorithm over various simulation durations, confirming its superior performance compared to traditional time-domain methods. This efficiency is particularly advantageous for long-duration simulations. The proposed approach provides a robust and efficient alternative for predicting motion responses in floating offshore wind turbines, combining high accuracy with improved computational performance. It represents a promising tool for enhancing the development and evaluation of offshore wind energy systems.



Academic Editor: Eugen Rusu

Received: 11 December 2024

Revised: 11 January 2025

Accepted: 14 January 2025

Published: 18 January 2025

Citation: Xu, J.; Li, C.; Jiang, W.; Lin, F.; Liu, S.; Lu, H.; Wang, H. Structural Response Prediction of Floating Offshore Wind Turbines Based on Force-to-Motion Transfer Functions and State-Space Models. *J. Mar. Sci. Eng.* **2025**, *13*, 160. <https://doi.org/10.3390/jmse13010160>

Copyright: © 2025 by the authors. Licensee MDPI, Basel, Switzerland. This article is an open access article distributed under the terms and conditions of the Creative Commons Attribution (CC BY) license (<https://creativecommons.org/licenses/by/4.0/>).

Keywords: floating offshore wind turbines; Cummins equation; transfer function; state-space model; wave frequency response prediction

1. Introduction

In recent years, renewable energy technologies have advanced significantly, with wind power playing a pivotal role in global initiatives to lower carbon emissions and shift towards sustainable energy sources. While conventional fixed-bottom offshore wind turbines have been successfully deployed worldwide, their expansion faces challenges in deeper waters and regions with challenging seabed conditions [1]. To overcome these limitations, floating offshore wind turbines have become a compelling solution, providing the ability to capture wind energy in deeper offshore environments where wind resources are abundant and accessible [2]. Unlike fixed offshore wind turbines, the floating foundation allows turbines to be positioned far from shore, opening vast new areas for offshore wind energy development. However, the environment in deep and distant seas is more complex and harsh, which necessitates greater attention to the service safety of floating offshore wind turbines [3]. Good stability is essential for the safe operation of floating offshore wind turbines, making motion response prediction crucial to ensure their safety and reliability.

Several methods are available for predicting the motion response of floating offshore wind turbines, with the choice of method influenced by factors such as budget and time constraints, desired accuracy, and the stage of the design cycle [2]. Faraggiana et al. [4] have detailed the connections between fidelity, computational efficiency, and the various design stages of motion response prediction algorithms for floating offshore wind turbines. Among these methods, computational fluid dynamics (CFD) methods are high fidelity approaches that can accurately simulate the aerodynamic and hydrodynamic behaviors of offshore wind turbines [5]. The dynamic properties of offshore wind turbines vary with operational and environmental conditions, such as changes in tower stiffness due to rotor speed variations [6]. These factors can also be incorporated into the refined modeling of CFD. Consequently, researchers frequently employ CFD methods to analyze the dynamic performance of offshore wind turbines [7,8]. Li et al. [9] proposed a dynamic overset grid technology to simulate the NREL phase VI wind turbine, using CFD methods to determine aerodynamic parameters, including total power, thrust, sectional normal force, and local pressure. Cai et al. [10] employed CFD method to analyze the aerodynamic behavior of offshore wind turbines, highlighting the correlation between the drag force on the tower and the phase of combined surge–pitch motion, as well as the rotor thrust and its phase in relation to the combined surge–pitch motion. In addition to aerodynamics, the hydrodynamics of offshore wind turbines are essential to dynamic analysis, as the coupling of aerodynamic and hydrodynamic forces act on the turbines simultaneously. Dynamic performance analysis of offshore wind turbines, accounting for both wave and wind effects, can be conducted through fully coupled CFD simulations [11]. Tran and Kim [12] used CFD to simulate the fluid–structure interaction of an offshore wind turbine, incorporating the effects of aero-hydrodynamic coupling. Their results showed a strong correlation between aerodynamic loads and the motion of the floating platform. Zhou et al. [13] examined the influence of wave type and wave steepness on the hydro/aerodynamic performance of the floating offshore wind turbines using CFD. Their findings indicated that the aerodynamic performance of the turbine is minimally impacted by wave type and wave steepness, and that reconstructed focused waves can be used to simulate the hydrodynamic characteristics of extreme waves. Despite the high fidelity of CFD methods, the computational complexity poses significant challenges. The large scale of the structures leads to inefficient computation, making CFD methods less convenient for the improvement of offshore wind turbine design [14,15].

Different from the CFD method, which solves Navier–Stokes equations, the potential flow theory assumes that the fluid surrounding offshore wind turbines is inviscid, irrotational, and incompressible, simplifying the fundamental equations of fluid dynamics.

Under these assumptions, the motion prediction of large-sized floating offshore wind turbines using potential flow theory requires fewer computing resources. The first-order potential theory is typically applied to calculate the motion of floating offshore platforms subjected to wave force excitation [16,17]. The approach decomposes waves into single-frequency components and calculates the corresponding response amplitude operators (RAOs). The motion response can then be obtained by superposing these single-frequency components [18]. This approach is convenient and efficient for predicting the motion response of floating offshore wind turbines. However, RAOs are the quantities in frequency domain, meaning only steady-state motions responses can be obtained [19]. To capture the transient response of floating structures under the potential flow theory, Cummins [20] introduced an equation to govern the motion of floating structures, known as the Cummins equation, which utilizes a combination of added inertia force and a convolution integral related to the hydrodynamic parameters of floating offshore wind turbines to represent the radiation force. These hydrodynamic parameters can be determined using the frequency domain Green's function [21–23], making the Cummins equation an indirect time-domain method. Based on these hydrodynamic parameters, the added mass and retardation function in the Cummins equation can be calculated [24], compensating for the inability of transient response analysis. The Cummins equation combines the advantages of the fast computation of hydrodynamic coefficients in the frequency domain with the ability to perform transient analysis in the time domain, making it widely applied in the motion response analysis of floating offshore wind turbines [25–27]. To obtain the motion response of floating offshore wind turbines, numerical methods are commonly used to obtain the solution to the Cummins equation. However, when solving the Cummins equation using numerical integration methods, each step involves the time-consuming process of convolving the velocity at the current time step with the retardation function from previous time steps [8], which also makes the development of standardized calculation packages more difficult [28].

To address the computational challenges of the convolution integral and improve efficiency, various studies have proposed solutions that can be categorized into two principal types: frequency or Laplace domain methods and state-space methods. In the frequency or Laplace domain, convolution terms are transformed into product terms, simplifying the complex convolution integral. The motion response of floating offshore wind turbines can subsequently be determined by employing the inverse Fourier or Laplace transform. Unlike the vibrating equation of fixed offshore structures, the velocity coefficients of floating offshore structures are frequency-dependent or relative to Laplace variable. To analytically represent these coefficients, Liu et al. [29] used a complex exponential to represent the retardation function and obtained an analytical solution of the retardation function in the Laplace domain. Using the Laplace transform, the frequency response of floating structures is determined, eliminating the need for convolution term calculations. Lu et al. [19] proposed an approach using poles and residues to analyze the floating structure response. Through the application of the Laplace transform to the Cummins equation and the calculation of transfer function poles and residues, they were able to accurately evaluate the dynamic behavior of floating offshore wind turbines while avoiding the accumulative errors associated with convolution integrals. On the other hand, statespace model-based methods effectively handle convolution term calculations. Perez and Fossen [30] applied state-space models to estimate the convolution terms, using frequency domain methods to determine the parameters from frequency-dependent hydrodynamic parameters. Taghipour et al. [8] summarized methods for analyzing the dynamic response of floating structures applying state-space approaches, including the transformation of convolution terms into a state-space formulation and the use of a state-space model for the force-to-motion re-

sponse. Although they presented three methods for estimating the state-space models of convolution terms, they did not describe methods for estimating state-space models associated with force-to-motion responses. Lu et al. [31] proposed a method to estimate the state-space models corresponding to the force-to-motion response of floating structures, applying it to the motion calculation of an offshore wind turbine. While these studies have addressed the convolution integral problem, some deficiencies remain. For example, when using Fourier or Laplace transform methods to determine the motion of floating offshore wind turbines, transient responses cannot be obtained, or the excitation needs to be linear. Additionally, methods using state-space models to substitute the force-to-motion response cannot compute the response induced by the initial conditions, such as displacement and velocity, in offshore wind turbines.

Unlike the methods mentioned above, the purpose of this research is to construct state-space models corresponding to the force-to-motion transfer relationship and build a computational framework for the transient response resulting from initial displacement and velocity of floating offshore wind turbines. The goal of this approach is to assess the motion response due to both the exciting force and initial conditions. Different from the traditional time or frequency domain methods, the primary objective of the study is to develop an efficient and accurate dynamic response calculation method that addresses the limitations of time-domain methods, such as error accumulation and low computational efficiency, as well as the frequency-domain methods, which can only compute steady-state responses. The algorithm initially utilizes the Laplace transform for the Cummins equation, obtaining the transfer functions for force-to-motion and initial conditions-to-motion. Next, the coefficients of the rational fraction related to the transfer functions are determined via a frequency domain fitting method. Based on the obtained coefficients, the state-space models associated with the force-to-motion relationship are constructed, and the transient motion responses resulting from initial conditions are expressed using a pole-residue form. The proposed method uses state-space models to calculate the response induced by external load and employ poles and residues to account for the response caused by initial conditions, thereby avoiding convolution calculations and significantly improving both computational efficiency and accuracy. The performance of the proposed method was validated using two numerical models. The first case involves a simple single degree of freedom (SDOF) system with an analytical solution, which was used to demonstrate the process and validate the proposed algorithm. The second example features a spar-type floating offshore wind turbine, employed to assess the accuracy and computational efficiency of the proposed algorithm.

2. Materials and Methods

2.1. Preliminaries

2.1.1. Laplace Transform

Laplace transform is one of the most commonly used methods in the domain of dynamic analysis. For a vibrating signal $x(t)$, the corresponding Laplace transform can be expressed as follows:

$$\tilde{x}(s) = \mathcal{L}[x(t)] = \int_0^{\infty} x(t)e^{-st} dt, \quad t \geq 0 \quad (1)$$

where $\mathcal{L}[\cdot]$ donates the Laplace transform, and s is the Laplace variable.

The motion governing equation of floating offshore wind turbines typically involves the velocity and acceleration of floating foundation. The properties of Laplace transform can be utilized to establish the connection as follows:

$$\mathcal{L}[\dot{x}(t)] = s\tilde{x}(s) - x(0) \quad (2)$$

$$\mathcal{L}[\ddot{x}(t)] = s^2\tilde{x}(s) - sx(0) - \dot{x}(0) \tag{3}$$

where $\dot{x}(t)$ and $\ddot{x}(t)$ are the first and second derivative of displacement, respectively, and $x(0)$ and $\dot{x}(0)$ are the initial conditions.

2.1.2. Parameter Estimation of Transfer Function Using Frequency-Domain Regression Fitting Method

The motion of floating offshore wind turbines can be modeled as the output of a system, with the transfer function describing the association between the system’s inputs and outputs. In control theory, the transfer function can be represented using a rational fraction as follows:

$$H(s) = \frac{P(s)}{Q(s)} = \frac{p_m s^m + p_{m-1} s^{m-1} + \dots + p_0}{s^n + q_{n-1} s^{n-1} + \dots + q_1 s + q_0} \tag{4}$$

where p_m, p_{m-1}, \dots, p_0 and $q_{n-1}, q_{n-2}, \dots, q_0$ are the polynomial coefficients in the numerator and denominator of the rational fraction, respectively.

Generally, the discrete transfer function can be calculated using numerical method or estimated through experimental methods. To represent the system as a rational fraction, it is necessary to estimate the coefficients of the numerator and denominator polynomials. These coefficients are typically unknown and can be represented using a function of discrete transfer function as follows:

$$\hat{H}(s) = \frac{P(s, \theta)}{Q(s, \theta)} = \frac{\hat{p}_m s^m + \hat{p}_{m-1} s^{m-1} + \dots + \hat{p}_0}{s^n + \hat{q}_{n-1} s^{n-1} + \dots + \hat{q}_1 s + \hat{q}_0} \tag{5}$$

where

$$\theta = \left[\hat{p}_m \quad \hat{p}_{m-1} \quad \dots \quad \hat{p}_0 \quad \hat{q}_{n-1} \quad \dots \quad \hat{q}_1 \quad \hat{q}_0 \right] \tag{6}$$

The estimation of vector θ involves solving a nonlinear fitting problem. This requires finding a series of coefficients that minimizes the discrepancy between the known discrete transfer function and the values calculated using the rational fraction model. To simplifying the fitting process, a weighted fitting method can be employed. This approach converts the nonlinear least-squares problem into a quasi-linear regression issue. The fitting method involves using iterative weighting coefficients to refine the estimate of θ as follows:

$$\theta' = \min_{\theta} \sum_l s_{l,N-1} |Q(i\omega_l, \theta_N)H(i\omega_l) - P(i\omega_l, \theta_N)|^2 \tag{7}$$

in which

$$s_{l,N-1} = \frac{1}{Q(i\omega_l, \theta_{N-1})} \tag{8}$$

where $s_{l,N-1}$ is the weighting coefficient, N is the iteration number, and l is the index for discrete frequency. Since the initial $Q(i\omega_l, \theta_{N-1})$ is unknown, $s_{l,0}$ is typically set to 1 to operate the quasi-linear regression. After several iterations, the vector θ will converge to values that minimize the discrepancy between the known discrete transfer function and the rational fraction model. This iterative process results in the estimation of the polynomial coefficients in the numerator and denominator.

2.2. Motion Prediction of Floating Offshore Wind Turbines Using State-Space Model

2.2.1. Motion Governing Equation of Floating Offshore Wind Turbines in Time and Laplace Domain

In order to describe the motion of floating offshore wind turbine structure, potential theory is applied to calculate the hydrodynamic, with the assumption of an ideal fluid. The

motion behavior of floating offshore wind turbines can be represented by the Cummins equation [32]:

$$(\mathbf{M} + \mathbf{M}_a)\ddot{\mathbf{x}}(t) + \int_0^t \mathbf{K}(t - \tau)\dot{\mathbf{x}}(\tau)d\tau + \mathbf{B}\mathbf{x}(t) + \mathbf{C}\mathbf{x}(t) = \mathbf{f}(t) \tag{9}$$

where \mathbf{M} is the mass matrix; \mathbf{M}_a and $\mathbf{K}(t)$ are the added mass matrix and retardation function matrix, which are associated with the radiation potential; \mathbf{B} is the viscous damping matrix; \mathbf{C} is the restoring matrix; $\mathbf{x}(t)$, $\dot{\mathbf{x}}(t)$, and $\ddot{\mathbf{x}}(t)$ are the displacement, velocity, and acceleration of floating offshore wind turbines; and $\mathbf{f}(t)$ refers to the wave force related to the incident and diffraction potential.

Equation (9) describes the motion dynamics of floating offshore wind turbines. However, the presence of the convolution term makes it inconvenient to solve the Cummins equation using numerical methods, buildup reduced computational efficiency, and significant accumulated error [33]. In order to address these issues, the Laplace transform is performed on Equation (9), obtaining the following formula in the Laplace domain:

$$(\mathbf{M} + \mathbf{M}_a) \left[s^2\tilde{\mathbf{x}}(s) - s\mathbf{x}_0 - \mathbf{v}_0 \right] + \tilde{\mathbf{K}}(s) \left[s\tilde{\mathbf{x}}(s) - \mathbf{x}_0 \right] + s\mathbf{B}\tilde{\mathbf{x}}(s) + \mathbf{C}\tilde{\mathbf{x}}(s) = \tilde{\mathbf{f}}(s) \tag{10}$$

where \mathbf{x}_0 and \mathbf{v}_0 are the initial conditions of floating offshore wind turbines, $\tilde{\mathbf{x}}(s)$ and $\tilde{\mathbf{f}}(s)$ correspond to the Laplace transform of $\mathbf{x}(t)$ and $\mathbf{f}(t)$, respectively.

Rewriting Equation (10), the following expression can be obtained:

$$\mathbf{Z}(s)\tilde{\mathbf{x}}(s) = \tilde{\mathbf{f}}(s) + \left[s(\mathbf{M} + \mathbf{M}_a) + \tilde{\mathbf{K}}(s) \right] \mathbf{x}_0 + (\mathbf{M} + \mathbf{M}_a)\mathbf{v}_0 + \mathbf{B}\mathbf{x}_0 \tag{11}$$

where $\mathbf{Z}(s)$ is the impedance function, expressed as:

$$\mathbf{Z}(s) = s^2(\mathbf{M} + \mathbf{M}_a) + s \left[\tilde{\mathbf{K}}(s) + \mathbf{B} \right] + \mathbf{C} \tag{12}$$

Based on Equation (11), the motion of floating offshore wind turbines can be viewed as resulting from wave force, initial displacement and velocity, respectively. The left part of the equation is connected to the motion response and the system involving floating offshore wind turbines and the surrounding fluid. The right part of the equation includes contributions from the wave force, initial displacement and velocity. By separating these contributions, one can analyze the effects of each component on the dynamic response of the system.

To calculate the motion response, the Laplace transform of displacement is expressed as the following:

$$\tilde{\mathbf{x}}(s) = \mathbf{H}_1(s)\tilde{\mathbf{f}}(s) + \mathbf{H}_2(s)[(\mathbf{M} + \mathbf{M}_a)\mathbf{v}_0 + \mathbf{B}\mathbf{x}_0] + \mathbf{H}_3(s)(\mathbf{M} + \mathbf{M}_a)\mathbf{x}_0 + \mathbf{H}_3(s)\mathbf{x}_0 \tag{13}$$

where

$$\mathbf{H}_1(s) = \frac{1}{\mathbf{Z}(s)} \tag{14}$$

$$\mathbf{H}_2(s) = \frac{s}{\mathbf{Z}(s)} = s\mathbf{H}_1(s) \tag{15}$$

$$\mathbf{H}_3(s) = \frac{\tilde{\mathbf{K}}(s)}{\mathbf{Z}(s)} = \tilde{\mathbf{K}}(s)\mathbf{H}_1(s) \tag{16}$$

$\mathbf{H}_1(s)$, $\mathbf{H}_2(s)$, and $\mathbf{H}_3(s)$ are the transfer functions, illustrating the relation between inputs and outputs of the system. According to Equations (13)–(16), the motion response of

floating offshore wind turbines can be obtained using transfer functions and system inputs, which include wave force and initial displacement and velocity.

2.2.2. Cummins Equation in Frequency Domain and Transform Function Decoupling

To predict the dynamic motion of floating offshore wind turbines, obtaining the transfer functions is essential. However, the irregularity of the wet surface on floating offshore wind turbines makes it challenging to derive analytical expressions for these transfer functions. Instead, the hydrodynamic parameters of floating offshore wind turbines are typically calculated with numerical methods, which results in discrete values for these parameters. To establish the connection between the transfer function and the hydrodynamic parameters, the Fourier transform is applied to Equation (9). This leads to the following expression for the Cummins equation in the frequency domain:

$$-\omega^2(M + M_a)\tilde{x}(i\omega) + i\omega\tilde{K}(i\omega)\tilde{x}(i\omega) + i\omega B\tilde{x}(i\omega) + C\tilde{x}(i\omega) = \tilde{f}(i\omega) \tag{17}$$

where ω denotes the radian frequency of incident wave, i denotes the imaginary unit; $\tilde{x}(i\omega)$, $\tilde{K}(i\omega)$, and $\tilde{f}(i\omega)$ denote the Fourier transform of retardation function and wave force, respectively.

The frequency domain representation allows for the transfer functions to be derived from the hydrodynamic parameters, making it possible to calculate the motion response efficiently using numerical methods. According to Euler’s formula, the relationship below can be obtained:

$$\tilde{K}(i\omega) = \int_{-\infty}^{\infty} K(t)e^{-i\omega t} dt = K^R(\omega) - iK^I(\omega) \tag{18}$$

in which

$$K^R(\omega) = \int_{-\infty}^{\infty} K(t) \cos \omega t dt \tag{19}$$

$$K^I(\omega) = \int_{-\infty}^{\infty} K(t) \sin \omega t dt \tag{20}$$

where $K^R(\omega)$ and $K^I(\omega)$ represent the real and imaginary part of $\tilde{K}(i\omega)$, respectively.

Substituting Equation (18) into Equation (17), the Cummins equation in the frequency domain is represented as the following:

$$-\omega^2[M + A(\omega)]\tilde{x}(i\omega) + i\omega[B(\omega) + B]\tilde{x}(i\omega) + C\tilde{x}(i\omega) = \tilde{f}(i\omega) \tag{21}$$

in which

$$A(\omega) = M_a - \frac{1}{\omega}K^I(\omega) = M_a - \frac{1}{\omega} \int_{-\infty}^{\infty} K(t) \sin \omega t dt \tag{22}$$

$$B(\omega) = K^R(\omega) = \int_{-\infty}^{\infty} K(t) \cos \omega t dt \tag{23}$$

where $A(\omega)$ and $B(\omega)$ represent the added mass potential damping, which can be calculated using hydrodynamic software.

According to Equation (22), the added mass matrix can be obtained by frequency-dependent added mass as follows:

$$M_a = \lim_{\omega \rightarrow \infty} A(\omega) = A(\infty) \tag{24}$$

Substituting Equations (22)–(24) into Equation (18), the following expression represents the Fourier transform of the retardation function using the hydrodynamic parameters of floating offshore wind turbines:

$$\tilde{K}(i\omega) = B(\omega) - i\omega[A(\infty) - A(\omega)] \tag{25}$$

Similarly, the impedance function can also be represented using hydrodynamic parameters:

$$Z(i\omega) = -\omega^2[M + A(\omega)] + i\omega[B(\omega) + B] + C \tag{26}$$

Substituting Equations (25) and (26) into Equations (14)–(16), the transfer functions expressed using radian frequency are obtained as follows:

$$H_1(i\omega) = \frac{1}{-\omega^2[M + A(\omega)] + i\omega[B(\omega) + B] + C} \tag{27}$$

$$H_2(i\omega) = \frac{i\omega}{-\omega^2[M + A(\omega)] + i\omega[B(\omega) + B] + C} \tag{28}$$

$$H_3(i\omega) = \frac{B(\omega) - i\omega[A(\infty) - A(\omega)]}{-\omega^2[M + A(\omega)] + i\omega[B(\omega) + B] + C} \tag{29}$$

With reference to the hydrodynamic parameters of floating offshore wind turbines, the transfer functions that relate the inputs (wave force, initial displacement and velocity) to the motion response can be derived. These transfer functions are essential for calculating the motion response using state-space model.

It is evident that the transfer functions are coupled across different degrees of freedom, making the estimation of the corresponding state-space models impractical. To address this issue, it is necessary to implement decoupling processes for the transfer functions. According to Equations (27) and (28), the transfer functions are determined by the hydrodynamic parameters of floating offshore wind turbines. In practical hydrodynamic analysis, numerical methods are commonly used to compute the discrete hydrodynamic parameters, such as $A(\omega_l)$ and $B(\omega_l)$ for discrete frequencies $\omega_l (l = 1, 2, \dots, L)$.

Substituting the discrete hydrodynamic parameters $A(\omega_l)$ and $B(\omega_l)$ into Equations (27)–(29), the discrete transfer functions are obtained as follows:

$$H_1(i\omega_l) = [Z(i\omega_l)]^{-1} = \begin{bmatrix} Z_{11}(i\omega_l) & Z_{12}(i\omega_l) & \cdots & Z_{16}(i\omega_l) \\ Z_{21}(i\omega_l) & Z_{22}(i\omega_l) & \cdots & Z_{26}(i\omega_l) \\ \vdots & \vdots & \ddots & \vdots \\ Z_{61}(i\omega_l) & Z_{62}(i\omega_l) & \cdots & Z_{66}(i\omega_l) \end{bmatrix}^{-1} \tag{30}$$

$$H_2(i\omega_l) = [Z(i\omega_l)]^{-1} = i\omega_l \begin{bmatrix} Z_{11}(i\omega_l) & Z_{12}(i\omega_l) & \cdots & Z_{16}(i\omega_l) \\ Z_{21}(i\omega_l) & Z_{22}(i\omega_l) & \cdots & Z_{26}(i\omega_l) \\ \vdots & \vdots & \ddots & \vdots \\ Z_{61}(i\omega_l) & Z_{62}(i\omega_l) & \cdots & Z_{66}(i\omega_l) \end{bmatrix}^{-1} \tag{31}$$

$$H_3(i\omega) = \tilde{K}(i\omega)[Z(i\omega)]^{-1} = \begin{bmatrix} \tilde{K}_{11}(i\omega_l) & \tilde{K}_{12}(i\omega_l) & \cdots & \tilde{K}_{16}(i\omega_l) \\ \tilde{K}_{21}(i\omega_l) & \tilde{K}_{22}(i\omega_l) & \cdots & \tilde{K}_{26}(i\omega_l) \\ \vdots & \vdots & \ddots & \vdots \\ \tilde{K}_{61}(i\omega_l) & \tilde{K}_{62}(i\omega_l) & \cdots & \tilde{K}_{66}(i\omega_l) \end{bmatrix}^{-1} \begin{bmatrix} Z_{11}(i\omega_l) & Z_{12}(i\omega_l) & \cdots & Z_{16}(i\omega_l) \\ Z_{21}(i\omega_l) & Z_{22}(i\omega_l) & \cdots & Z_{26}(i\omega_l) \\ \vdots & \vdots & \ddots & \vdots \\ Z_{61}(i\omega_l) & Z_{62}(i\omega_l) & \cdots & Z_{66}(i\omega_l) \end{bmatrix}^{-1} \tag{32}$$

where $Z_{jk}(i\omega_l)$ and $\tilde{K}_{jk}(i\omega_l)$ $j = 1, 2, \dots, 6; k = 1, 2, \dots, 6$ are the element of $\mathbf{Z}(i\omega_l)$ and $\tilde{\mathbf{K}}(i\omega)$, respectively.

According to Equations (30)–(32), the discrete transfer functions have been calculated, indicating that the transfer functions are decoupled. The next phase involves estimating the corresponding state-space model from these discrete transfer functions.

2.2.3. Parameters of State-Space Model Estimation

According to Equation (13), the first component on the right-hand side denotes the response caused by wave force, while the last three terms are corresponding to the response due to initial displacement and velocity. Performing the inverse Laplace transform on Equation (13) yields the motion response of offshore wind turbines, as shown below:

$$x(t) = \int_0^t h_1(\tau)f(t - \tau)d\tau + h_1(t)[(\mathbf{M} + \mathbf{M}_a)v_0 + \mathbf{B}x_0] + h_2(t)(\mathbf{M} + \mathbf{M}_a)x_0 + h_3(t)x_0 \quad (33)$$

where $h_1(t)$, $h_2(t)$, $h_3(t)$ are the inverse Laplace transform of $\mathbf{H}_1(s)$, $\mathbf{H}_2(s)$, $\mathbf{H}_3(s)$, respectively. These reflect the corresponding impulse response function.

According to the control theory, the impulse response function is represented in terms of a state-space model, where the convolution term is treated as the system’s output. To illustrate this, consider a single element from the first term of Equations (13) and (33) for simplicity. The following expression represents the motion response caused by wave force:

$$x(t) = \int_0^t h_1(\tau)f(t - \tau)d\tau \quad (34)$$

Here, $x(t)$ is an element of $x(t)$, $h_1(\tau)$ is a component of $h_1(t)$, and $f(t)$ is a component of $f(t)$ (the wave force input). This convolution integral provides the motion response due to wave forces by combining the impulse response with the input force over time.

A system’s transfer function is given by the ratio of the Laplace transform of the output to the Laplace transform of the input. It is given by the following equation:

$$H_1(s) = \frac{\tilde{x}(s)}{\tilde{f}(s)} = \frac{p_m s^m + p_{m-1} s^{m-1} + \dots + p_0}{s^n + q_{n-1} s^{n-1} + \dots + q_1 s + q_0} \quad (35)$$

where $H_1(s)$, $\tilde{x}(s)$ and $\tilde{f}(s)$ are the element of $\mathbf{H}_1(s)$, $\tilde{\mathbf{x}}(s)$ and $\tilde{\mathbf{f}}(s)$.

Because the highest order of the element of impedance function is second-order, the transfer function of the system has a relative degree of 2, which implies that the order n of the transfer function is $m + 2$. Based on Equations (5)–(8) and the discrete transfer functions, the parameters of the numerator and denominator polynomials of the rational fraction can be estimated. This process involves fitting the discrete data to determine the coefficients of the transfer function.

According to Equation (35), the transfer function can be formulated in the following pole-residue form:

$$H_1(s) = \frac{\tilde{x}(s)}{\tilde{f}(s)} = \sum_{j=1}^n \frac{\gamma_j}{s - \lambda_j} \quad (36)$$

where λ_j and γ_j are the poles and residues of the transfer function. It is obviously that the roots of $s^n + q_{n-1} s^{n-1} + \dots + q_1 s + q_0 = 0$ are the poles, and the corresponding residues are calculated using $\gamma_j = \lim_{s \rightarrow \lambda_j} (s - \lambda_j) H_1(s)$.

Based on Equation (36), the Laplace transform of the system’s output is determined by the poles and residues as follows:

$$\tilde{x}(s) = \sum_{j=1}^n \frac{\gamma_j}{s - \lambda_j} \tilde{f}(s) = \sum_{j=1}^n \gamma_j Z_j(s) \tag{37}$$

and the Laplace transform of the input to the system is given by:

$$\tilde{f}(s) = sZ_j(s) - \lambda_j Z_j(s) \tag{38}$$

where $Z_j(s)$ is a auxiliary variable.

Implementing inverse Laplace transform to Equations (37) and (38), the following expressions give the output and input of the system in the time domain:

$$x(t) = \sum_{j=1}^n \gamma_j z_j(t) \tag{39}$$

$$f(t) = \dot{z}_j(t) - \lambda_j z_j(t) \tag{40}$$

where $z_j(t)$ corresponds to the inverse Laplace transform of $Z_j(s)$.

To describe the connection between the output and input of the system in matrix form using a state-space model, Equations (39) and (40) can be converted as follows:

$$\begin{cases} \dot{z}(t) = \mathcal{A}z(t) + \mathcal{B}f(t) \\ x(t) = \mathcal{C}z(t) \end{cases} \tag{41}$$

where

$$z(t) = \begin{bmatrix} z_1(t) \\ z_2(t) \\ \vdots \\ z_n(t) \end{bmatrix}, \mathcal{A} = \begin{bmatrix} \lambda_1 & & & \\ & \lambda_2 & & \\ & & \ddots & \\ & & & \lambda_n \end{bmatrix}, \mathcal{B} = \begin{bmatrix} 1 \\ 1 \\ \vdots \\ 1 \end{bmatrix}, \mathcal{C} = [\gamma_1 \quad \gamma_2 \quad \cdots \quad \gamma_n] \tag{42}$$

The matrices \mathcal{A} , \mathcal{B} , and \mathcal{C} construct the state-space model corresponding to an element of the transfer function $H_1(s)$. Utilizing the state-space model, the motion response of the floating offshore wind turbine induced by wave force can be further determined.

2.2.4. Motion Response Calculation of Floating Offshore Wind Turbines

The motion response caused by wave force can be considered as the system’s output based on the estimated state-space model. Meanwhile, the motion response of floating offshore wind turbines due to initial displacement and velocity is also a part of the total response. According to Equation (33), the motion due to initial conditions is related to the impulse response functions of $h_2(t)$ and $h_3(t)$. To calculate the function of $h_2(t)$, the element of $H_1(s)$ is substituted into Equation (15)

$$H_2(s) = sH_1(s) = \frac{\hat{p}_m s^{m+1} + \hat{p}_{m-1} s^m + \cdots + \hat{p}_0 s}{s^n + \hat{q}_{n-1} s^{n-1} + \cdots + \hat{q}_1 s + \hat{q}_0} \tag{43}$$

And then, the element of the transfer function $H_2(s)$ can be represented in pole-residue form as shown below:

$$H_2(s) = \sum_{j=1}^n \frac{\delta_j}{s - \lambda_j} \tag{44}$$

where δ_j is the residue, which is calculated by the limitation of $\delta_j = \lim_{s \rightarrow \lambda_j} (s - \lambda_j) H_2(s)$.

Unlike $H_2(s)$, the transfer function $H_3(s)$ is related to $\tilde{K}(s)$ and $H_1(s)$ based on Equation (16). $\tilde{K}(s)$ can also be represented by a rational fraction with a relative degree of 1 [8]. Considering that the relative degree of the rational fraction of $H_1(s)$ is 2, the relative degree of $H_3(s)$ is 3. Equations (5)–(8) are employed to determine the coefficients of the rational fraction of $H_3(s)$, and the element of $H_3(s)$ can be further written in pols-residue form as follows:

$$H_3(s) = \frac{\hat{a}_r s^r + \hat{a}_{r-1} s^{r-1} + \dots + \hat{a}_0}{s^{r+3} + \hat{b}_{r+2} s^{r+2} + \dots + b_1 s + \hat{b}_0} = \sum_{j=1}^{r+3} \frac{\mu_j}{s - \nu_j} \tag{45}$$

where μ_j and ν_j are the pole and residue of $H_3(s)$.

Implementing inverse Laplace transform to Equations (36), (44), and (45), the impulse response functions are obtained as follows:

$$h_1(t) = \sum_{j=1}^n \gamma_j e^{\lambda_j t} \tag{46}$$

$$h_2(t) = \sum_{j=1}^n \delta_j e^{\lambda_j t} \tag{47}$$

$$h_3(t) = \sum_{j=1}^{r+3} \mu_j e^{\nu_j t} \tag{48}$$

Substituting Equations (41) and (46)–(48) into Equation (33), the state-space model and impulse response functions can be used to determine the motion response of a floating offshore wind turbine, considering both wave force and initial conditions.

2.3. Execution Steps of Proposed Algorithm

To execute the proposed algorithm of structural response prediction of floating offshore wind turbines based on force-to-motion transfer functions and state-space models, the following steps are employed:

(1) The Laplace transform is applied to the Cummins equation using Equation (9) to obtain the impedance function of force-to-response, and the transfer functions of Equations (14)–(16) are calculated further, which are used to express the motion response in Laplace domain.

(2) Implementing inverse Laplace transform using Equation (33), the motion response of offshore wind turbines can be expressed by impulse response functions, which displays the relationship between wave force, initial conditions, and motion response.

(3) Applying Fourier transform to the Cummins equation and substituting the discrete hydrodynamic parameters of $A(\omega_l)$ and $B(\omega_l)$, the decoupling transfer functions can be obtained using Equations (30)–(32).

(4) Substituting the decoupling transfer functions into Equations (5)–(8), the corresponding transfer functions can be expressed using rational fraction.

(5) Based on the parameters of the rational fraction, the state-space models can be constructed using Equations (35)–(42), and the corresponding impulse response functions are calculated applying Equations (43)–(48).

(6) Substituting the estimated state-space models and impulse response functions into Equation (33), the motion responses induced by wave force and initial conditions are calculated.

The flow diagram of the proposed algorithm is shown as Figure 1. According to the procedures, the structural response of floating offshore wind turbines can be predicted.

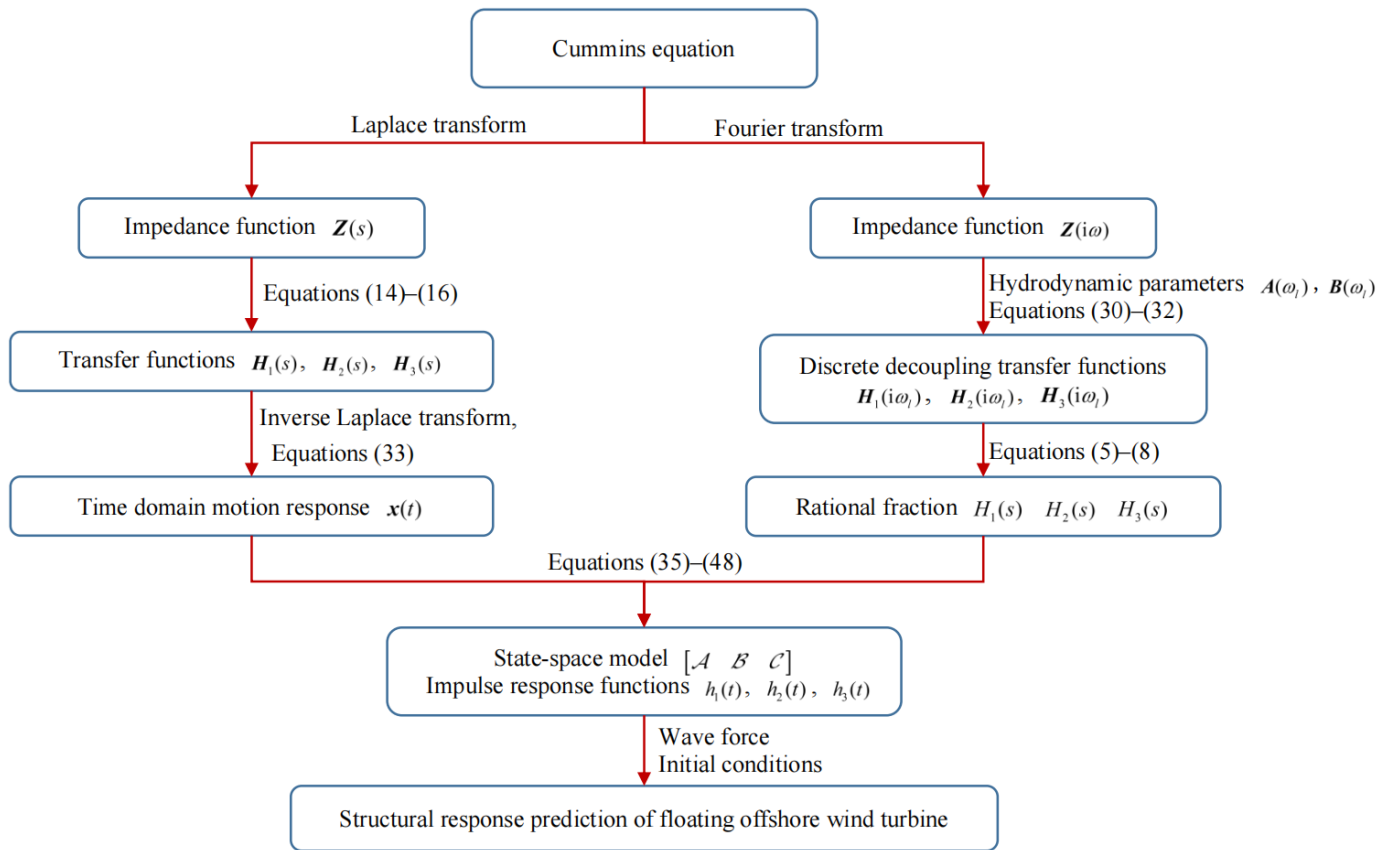


Figure 1. Flow diagram of the proposed algorithm.

3. Results

Two test cases, an SDOF system and a numerical model of spar-type floating offshore wind turbine, are applied to the proposed method. The results are compared with that of Newmark-β method to demonstrate the performance of the proposed method. The software MATLAB R2016b is utilized to implement the analysis process, including intermediate steps and motion response calculations.

3.1. Test Case: Analytical SDOF Model

To demonstrate the proposed algorithm, an analytical single degree of freedom (SDOF) model is applied initially. This model does not represent any practical system but symbolically signifies the uncoupled heave motion of floating offshore structures. The SDOF model is analytical, and the theoretical values corresponding to hydrostatic and hydrodynamic parameters are known. These theoretical values can be employed to validate the proposed algorithm.

3.1.1. Parameters of SDOF System

The motion governing equation for the SDOF system is similar in form to the Cummins equation and is given by the following:

$$(M + M_a)\ddot{x}(t) + \int_0^t K(t - \tau)\dot{x}(\tau)d\tau + B\dot{x}(t) + Cx(t) = \sum_{i=1}^N A_i \cos(2\pi f_i t + \phi_i) \quad (49)$$

where A_i , f_i and ϕ_i are the amplitude, frequency, and phase of exciting force; $M = 1$, $B = 5.5$, and $C = 8$.

The added mass and damping are defined using following formula

$$A(\omega) = \delta + \frac{(\alpha^2 + \beta^2 - \omega^2)(\beta - 1)}{(\alpha^2 + \beta^2 - \omega^2)^2 + 4\alpha^2\omega^2} \tag{50}$$

$$B(\omega) = \frac{2\alpha(\beta + 1)\omega^2}{(\alpha^2 + \beta^2 - \omega^2)^2 + 4\alpha^2\omega^2} \tag{51}$$

where $\alpha = 0.2$, $\beta = 2$, and $\delta = 0.5$.

According to Equations (24) and (25), the added mass of SDOF system is calculated as follows:

$$M_a = \lim_{\omega \rightarrow \infty} A(\omega) = \delta = 0.5 \tag{52}$$

and the Fourier transfer of the retardation function is given by the following:

$$\tilde{K}(i\omega) = \frac{3i\omega}{-\omega^2 + 0.4i\omega + 4.04} \tag{53}$$

Based on the connection $s = i\omega$, the corresponding Laplace transform is determined as shown below:

$$\tilde{K}(s) = \frac{3s}{s^2 + 0.4s + 4.04} \tag{54}$$

Equations (49)–(54) provide all the necessary information for the SDOF system. Each step of the proposed algorithm can be validated using the analytical solutions provided by this model, thereby demonstrating the validity and effectiveness of the proposed algorithm.

3.1.2. Transfer Functions Estimation Based on Discrete Hydrodynamic Parameters

Based on the given parameters of the SDOF system, the analytical transfer functions can be derived by employing Laplace transform to Equation (49) and substituting Equation (54) into the equation in the Laplace domain:

$$H_1(s) = \frac{1}{1.5s^2 + s\tilde{K}(s) + 5.5s + 8} = \frac{0.667s^2 + 0.2667s + 2.6933}{s^4 + 0.7333s^3 + 11.5067s^2 + 3.48s + 21.5467} \tag{55}$$

$$H_2(s) = \frac{s}{1.5s^2 + s\tilde{K}(s) + 5.5s + 8} = \frac{0.667s^3 + 0.2667s^2 + 2.6933s}{s^4 + 0.7333s^3 + 11.5067s^2 + 3.48s + 21.5467} \tag{56}$$

$$H_3(s) = \frac{\tilde{K}(s)}{1.5s^2 + s\tilde{K}(s) + 5.5s + 8} = \frac{2s}{s^4 + 0.7333s^3 + 11.5067s^2 + 3.48s + 21.5467} \tag{57}$$

In practical engineering calculations, only discrete hydrodynamic parameters are typically available due to limitations in experiments or numerical computations. For the SDOF system, the discrete added mass and damping are obtained from Equations (50) and (51), with a sampling interval frequency of $\Delta\omega = 0.01$ rad/s ranging from 0 to 20 rad/s. These discrete hydrodynamic parameters are plotted in Figure 2, corresponding to the known values used in the motion response analysis of the SDOF system.

To obtain the discrete transfer functions of the SDOF system, the discrete hydrodynamic parameters are substituted into Equations (27)–(29). These transfer functions are then represented as rational functions with polynomials in the numerator and denominator. To estimate the coefficients of these polynomials, the frequency-domain regression fitting method is applied. During this process, the discrete transfer functions are substituted into Equations (5)–(8), and the row vector θ , which consists the coefficients of the rational fraction, is calculated after several iterations.

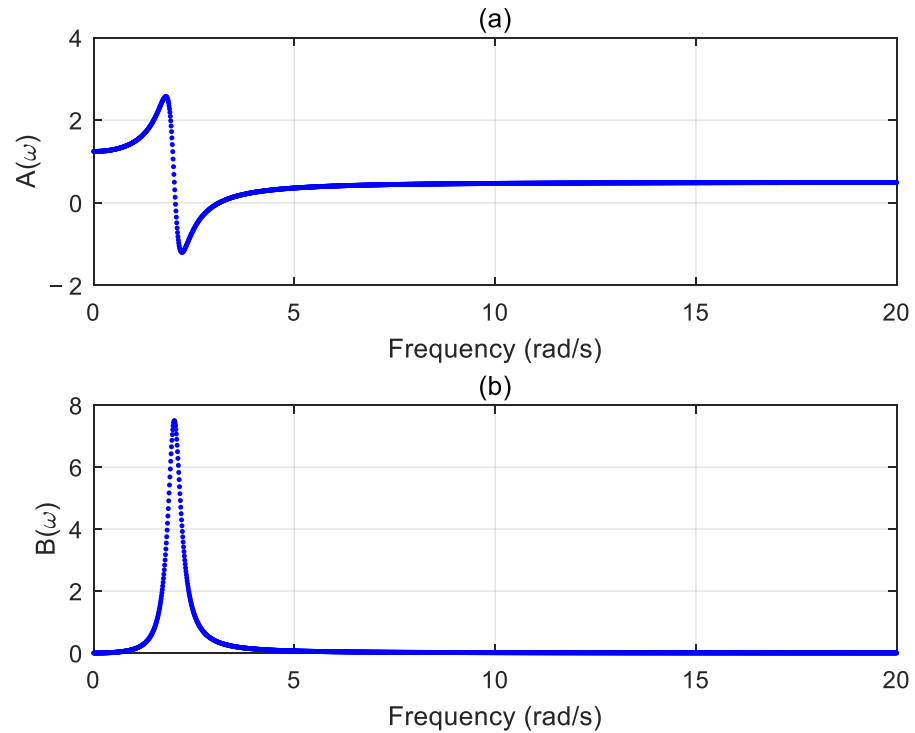


Figure 2. Discrete hydrodynamic parameters of SODF system: (a) added mass; and (b) damping.

For the discrete transfer function $H_1(i\omega)$, the denominator order is set to 4, and the estimated row vector of coefficients is $\hat{\theta}_1 = [0.6667, 0.2667, 2.6933, 0.7333, 11.5067, 3.48, 21.5467]$. Similarly, the coefficient vectors for $H_2(i\omega)$ and $H_3(i\omega)$ are estimated as $\hat{\theta}_2 = [0.6667, 0.2667, 2.6933, 0, 0.7333, 11.5067, 3.48, 21.5467]$ and $\hat{\theta}_3 = [2.0000, 0, 0.7333, 11.5067, 3.48, 21.5467]$, respectively. It is evident that the coefficients estimated using the proposed method perfectly align with the analytical values given in Equations (55)–(57), confirming the accuracy of the rational fraction estimation for the transfer functions.

To visually represent the results of the regression fitting method for estimating coefficients, the comparison plots for $H_1(s)$, $H_2(s)$, and $H_3(s)$ have been created, as shown in Figures 3–5. Firstly, the discrete added mass and damping are substituted into the expression of $H_1(s)$, $H_2(s)$, and $H_3(s)$ to calculate the corresponding discrete transfer functions, yielding a series of complex transfer functions across varying frequencies. Secondly, the regression fitting method is applied to this frequency series and corresponding complex transfer functions to estimate the transfer functions expressed as rational fractions. Thirdly, the frequency series are substituted into the estimated transfer functions, and the computed transfer functions are compared against the analytical values. As the transfer functions are complex, the comparison is plotted in the complex plane, with the horizontal x -axis representing the real part and the vertical y -axis representing the imaginary part. Based on Figures 3–5, the estimated transfer functions for $H_1(s)$, $H_2(s)$, and $H_3(s)$ closely match the analytical values. To quantitatively estimate the differences between the rational fraction and the theoretical transfer function, the root mean squared error (RMSE) of the real and imaginary parts of $H_1(s)$, $H_2(s)$, and $H_3(s)$ are calculated and listed in Table 1. The RMSE values approach zero, which means that the estimated transfer functions are accurate and can be used for further calculation of the corresponding motion response.

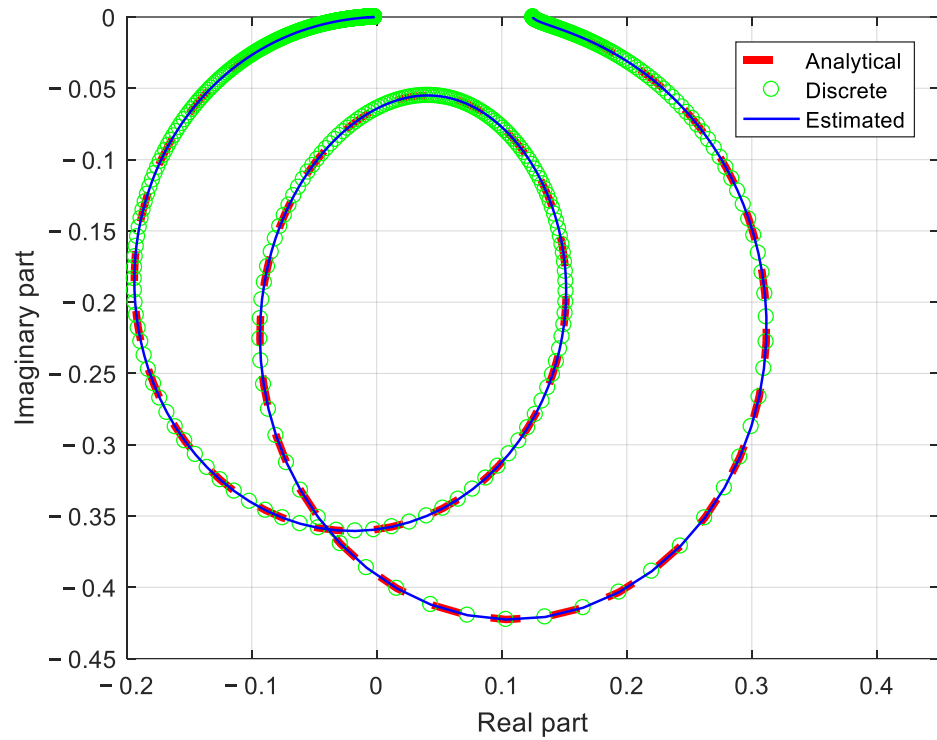


Figure 3. Comparison of the transfer function $H_1(s)$ between the analytical solution and the value determined by proposed algorithm.

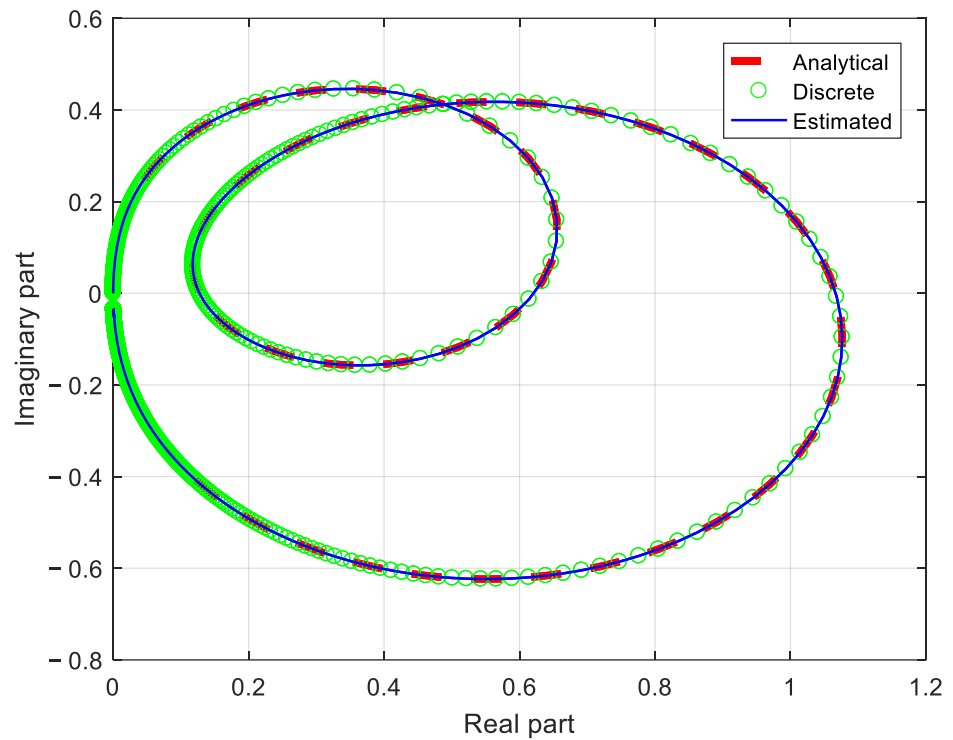


Figure 4. Comparison of the transfer function $H_2(s)$ between the analytical solution and the value determined by proposed algorithm.

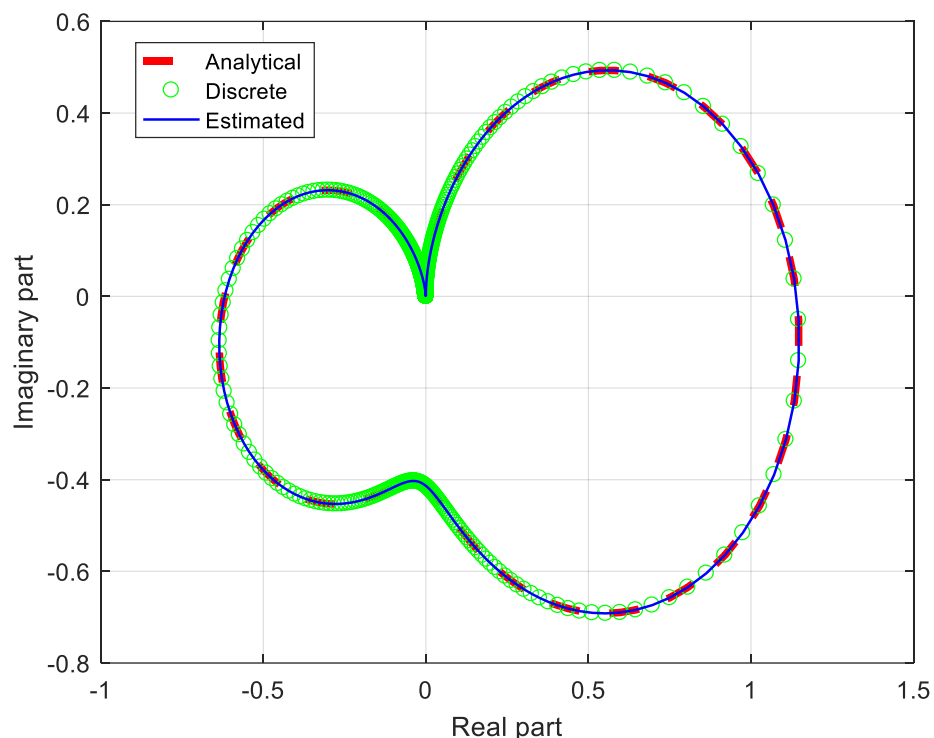


Figure 5. Comparison of the transfer function $H_3(s)$ between the analytical solution and the value determined by proposed algorithm.

Table 1. RMSE values of real and imaginary parts of $H_1(s)$, $H_2(s)$, and $H_3(s)$.

Transfer Function	Real Part	Image Part
$H_1(s)$	2.0179×10^{-14}	2.0177×10^{-14}
$H_2(s)$	1.1549×10^{-12}	1.1549×10^{-12}
$H_3(s)$	1.5132×10^{-15}	1.5164×10^{-15}

3.1.3. Calculation of the Motion Response for SDOF System

According to the regression fitting operation, the rational fraction of transfer functions $H_1(s)$, $H_2(s)$, and $H_3(s)$ have been obtained. These transfer functions correspond to the motion response of the SDOF model caused by initial conditions and wave force. The findings confirm that the estimated transfer functions accurately represent the system’s behavior, allowing for precise calculation of the motion response in the SDOF model.

Firstly, the effectiveness of the proposed algorithm in calculating the motion response caused by initial conditions is evaluated. According to Equation (33), the impulse response functions corresponding to $H_1(s)$, $H_2(s)$, and $H_3(s)$ need to be obtained to calculate the motion response due to initial displacement and velocity. After estimating the coefficients of the rational fractions for the transfer functions, the poles and residues are computed using Equations (36), (44), and (45). Subsequently, the impulse response functions are determined using Equations (46)–(48). The impulse functions of the SDOF system are depicted in Figure 6. Using these functions, the motion response due to the initial conditions is readily computed according to Equation (33).

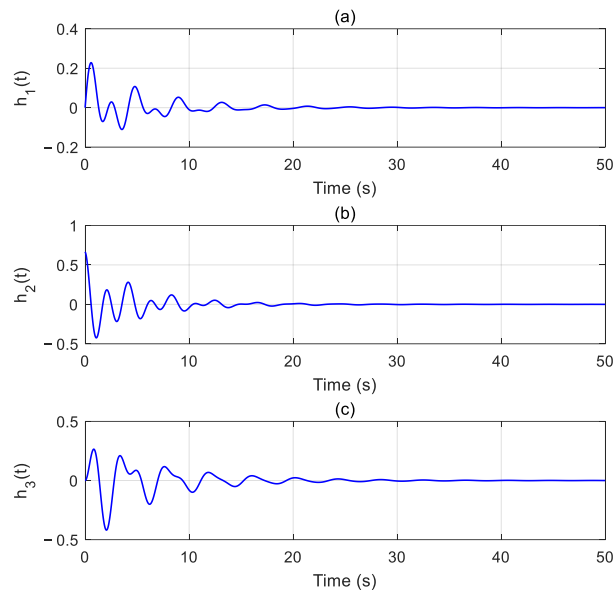


Figure 6. Impulse response functions of SDOF system: (a) $h_1(s)$ (b) $h_2(s)$ (c) $h_3(s)$.

To evaluate the effectiveness of the proposed algorithm, a comparison is made using the Newmark- β method. Unlike the proposed method, which relies on the transfer function approach, the Newmark- β method is a commonly used numerical technique for time-domain integration. This requires the retardation function to be determined beforehand. The retardation function can be calculated from the damping using the following formula [34]:

$$K(t) = \frac{\Delta\omega}{\pi} \sum_{n=1}^{N-1} 2B(n\Delta\omega) \cos(n\Delta\omega t) + \frac{\Delta\omega}{\pi} [B(0) + B(N) \cos(N\Delta\omega t)] \quad (58)$$

where $\Delta\omega$ is the frequency sampling interval. By inserting Equation (51) into the equation, the retardation function of the SDOF system is determined and shown as Figure 7. The figure demonstrates that the retardation function is a damped cosine curve, which will be involved in the convolution calculation within the Cummins equation.

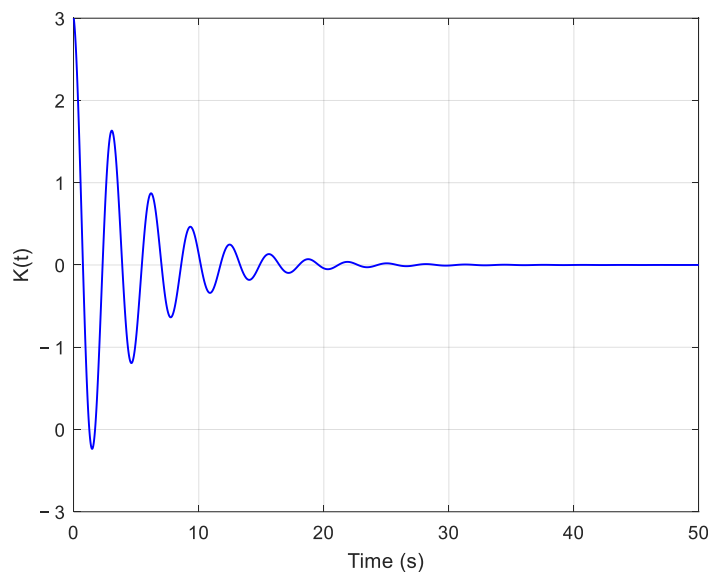


Figure 7. Retardation function of SDOF system.

When analyzing the motion response caused by initial conditions, the initial conditions of the SDOF system are set as $x_0 = 0.1$ m and $v_0 = 0.15$ m/s, respectively. Substituting these initial conditions along with the calculated impulse response functions into Equation (33), the motion response due to initial conditions is calculated. Similarly, the motion response is computed using the Newmark- β method with consistent initial conditions. The process of calculating the motion response of floating structures using the Newmark- β method can be found in reference [35]. Figure 8 shows the comparison of responses obtained from the two methods, which demonstrates that the response computed with the proposed algorithm closely matches the response achieved with the Newmark- β method, indicating that the proposed algorithm accurately computes the motion response due to initial conditions.

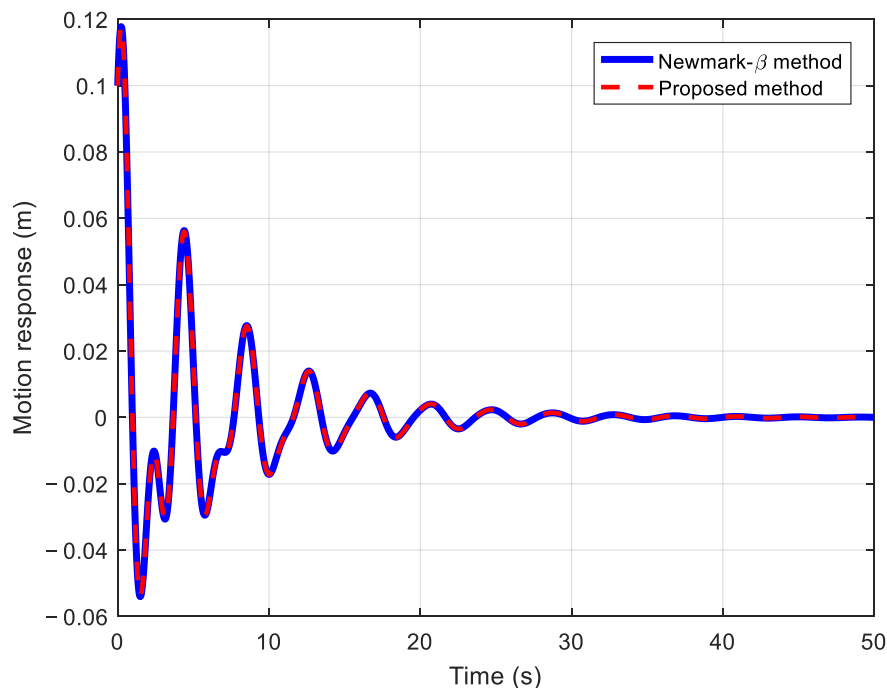


Figure 8. Comparison of motion response due to initial conditions using Newmark- β and proposed algorithm.

To better evaluate the proposed method’s performance, the SDOF system’s motion response is analyzed with both initial conditions and an applied exciting force. The initial conditions are set as in the previous analysis, and the exciting force is simulated using the formula on the right-hand side of Equation (49), with parameters provided in Table 2. The exciting force is plotted in Figure 9, based on the parameters.

Table 2. Parameters related to exciting force in Equation (49).

l	A_n	$\omega_l(\text{rad/s})$	ϕ_l
1	0.1728	0.1	0.9280
2	0.1812	0.5	0.1733
3	0.0400	1.2	-0.6916
4	0.1719	0.3	-0.7230
5	0.1592	0.28	-0.5744

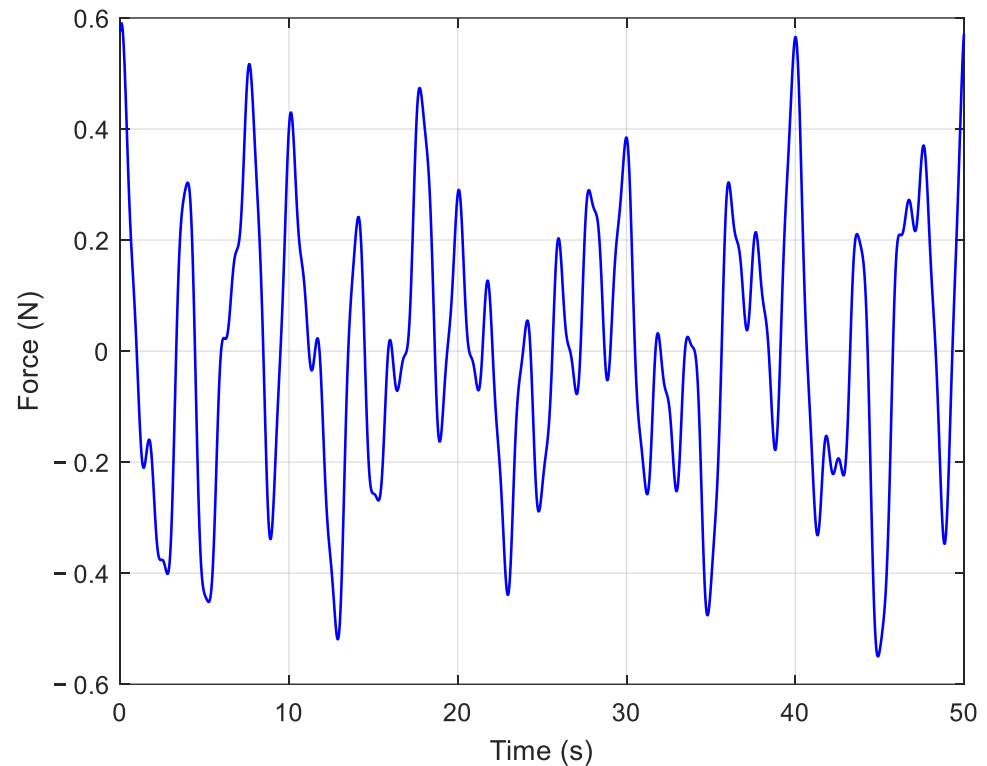


Figure 9. Exciting force acting on SDOF system.

For determining the motion response caused by the exciting force, the state-space model associated with transfer function $H_1(s)$ should be constructed. Using the estimated coefficients of the rational fraction, the poles and residues are determined via Equation (36), which are then used to construct the corresponding state-space model. For this system, the matrices are defined as follows: state matrix is $\mathcal{A} = \text{diag}[-0.2360 + 2.9883 I, -0.2360 - 2.9883 I, -0.1307 + 1.5430 I, -0.1307 - 1.5430 i]$, input matrix is $\mathcal{B} = [1, 1, 1, 1]^T$, and output matrix is $\mathcal{C} = [-0.0044 - 0.0837 I, -0.0044 + 0.0837 I, 0.0044 - 0.0537 I, 0.0044 + 0.0537 i]$.

The input to the state-space model is represented by the exciting force, which is then inserted into Equation (41) to determine the motion response resulting from this force. According to Equation (33), the total motion response is the sum of the response due to the initial conditions and the response due to the exciting force. To validate the proposed algorithm, comparison is carried out using the Newmark- β method. This method calculates the total motion response of the SDOF system under the combined influence of initial conditions and external loads. Figure 10 illustrates the comparison of responses obtained from both methods. Additionally, to further examine the comparison, the time-domain response is converted to the frequency domain, and the amplitude and phase comparison are presented in Figure 11. These figures demonstrated that the motion response of the SDOF system calculated using the proposed algorithm aligns well with the results from the Newmark- β method, both in the time and frequency domain. This indicates that the proposed algorithm can accurately compute the total motion response.

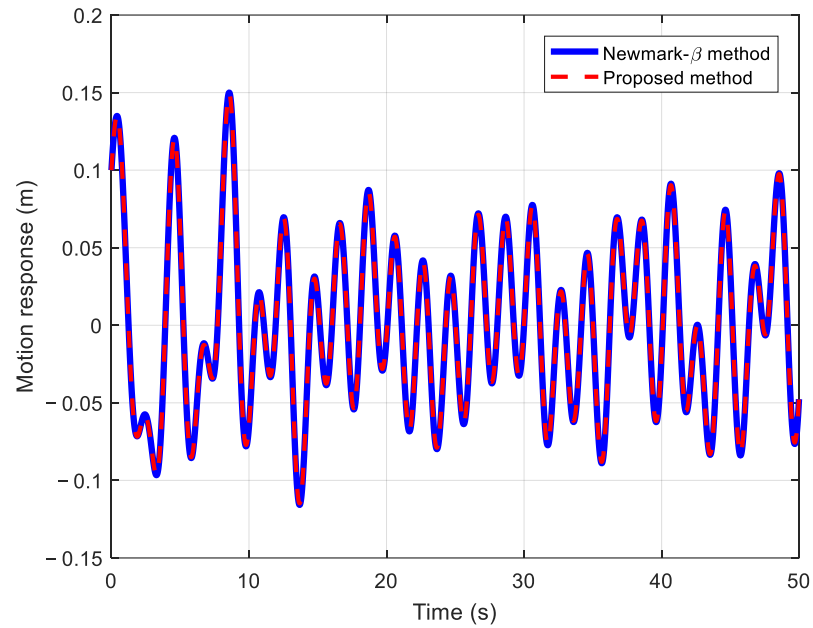


Figure 10. Total response comparison of SDOF system calculated by Newmark- β and proposed algorithm.

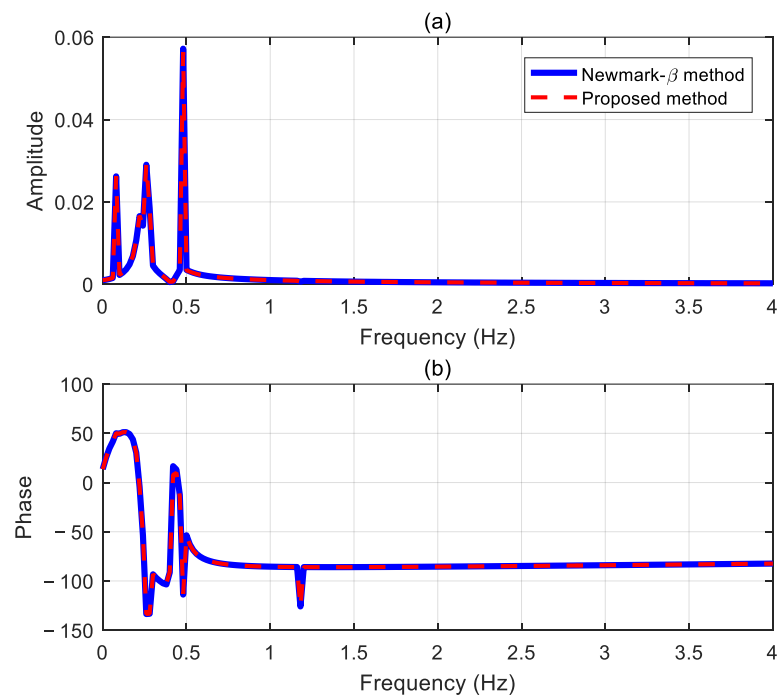


Figure 11. Total response comparison in frequency domain: (a) amplitude; and (b) phase.

3.2. Test Case: Floating Offshore Wind Turbine

A spar-type floating offshore wind turbine is utilized in this section to evaluate the proposed algorithm, with the Newmark- β method implemented for verification. The spar-type floating offshore wind turbine is a benchmark model developed by the National Renewable Energy Laboratory (NREL), which comprises an upper cylinder, a lower cylinder, and a conical frustum connecting them, with a draft of 120 m [36]. The tower, fixed atop the spar-type foundation, is situated 10 m above the still water level (SWL) at its base and extends to 87.6 m above the SWL. At the top of the tower, a 5 MW baseline wind turbine is

deployed. Jonkman [36] provides detailed parameters for the spar-type floating offshore wind turbine, whose structural model is shown in Figure 12a.

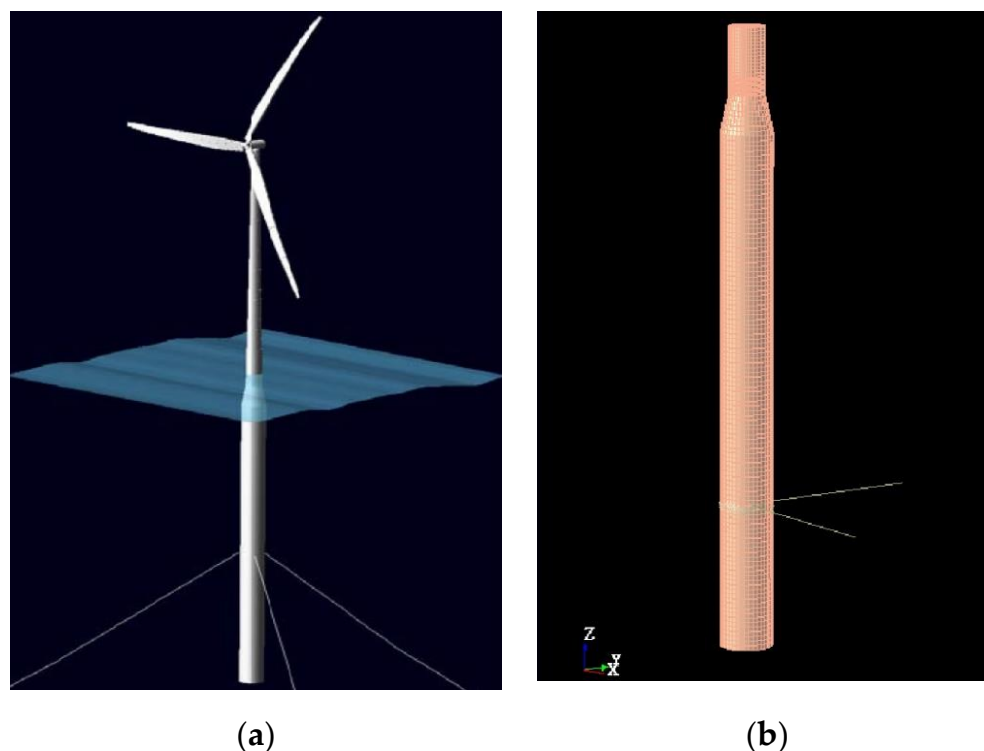


Figure 12. Structural model of spar-type floating offshore wind turbine: (a) structural model; (b) hydrodynamic model.

3.2.1. Hydrostatic and Hydrodynamic Parameters

To calculate the motion response of the floating offshore wind turbine, the hydrostatic and hydrodynamic parameters need to be obtained at first. The hydrodynamic model is established using commercial software, as shown in Figure 12b. The hydrostatic parameters of the floating offshore wind turbine, including the mass and restoring matrices, are calculated based on the center of buoyancy, center of gravity, and radius of gyration.

The hydrodynamic parameters for the added mass and potential damping of the floating offshore wind turbine are extracted using hydrodynamic analysis module. Due to the structural symmetry of the system, the hydrodynamic parameters exhibit the following relationships: $A_{11} = A_{22}$, $A_{44} = A_{55}$, $A_{15} = A_{51}$, and $A_{24} = A_{42}$. Similarly, the potential damping displays the same symmetry as the added mass. Consequently, both the added mass and potential damping can be represented as the real and imaginary components of the Fourier transform of the retardation function. The added mass and potential damping are plotted in Figures 13 and 14, with the frequency varying from 0.01 rad/s to 4.985 rad/s, with an interval of 0.015 rad/s.

The Newmark- β method is selected as the benchmark for assessing the proposed algorithm. To apply the Newmark- β method to the motion prediction of the floating offshore wind turbine, the retardation function needs to be determined, which is derived from the discrete potential damping using Equation (58). The calculated retardation function is plotted in Figure 15, illustrating its behavior over the specified frequency range.

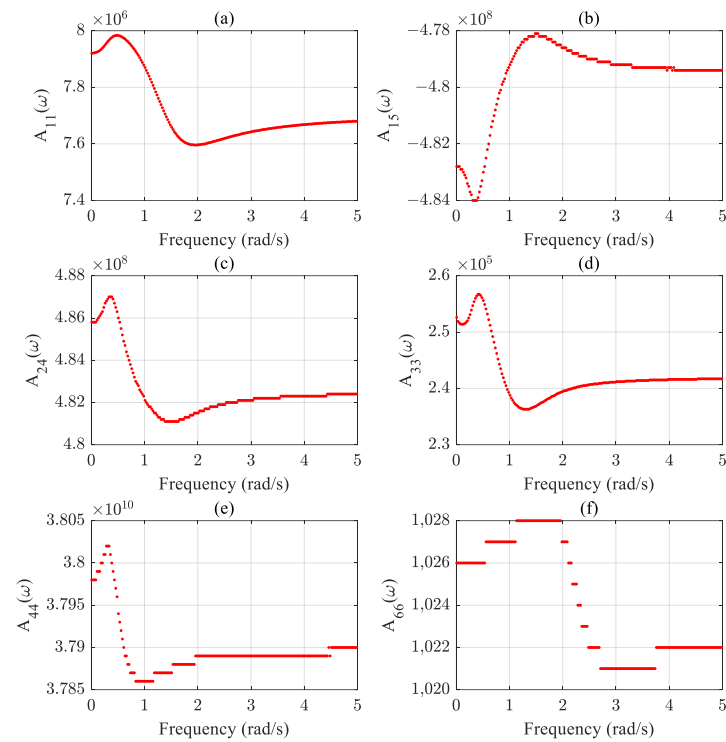


Figure 13. Added mass for floating offshore wind turbine: (a) $A_{11}(\omega)$; (b) $A_{15}(\omega)$; (c) $A_{24}(\omega)$; (d) $A_{33}(\omega)$; (e) $A_{44}(\omega)$; and (f) $A_{66}(\omega)$.

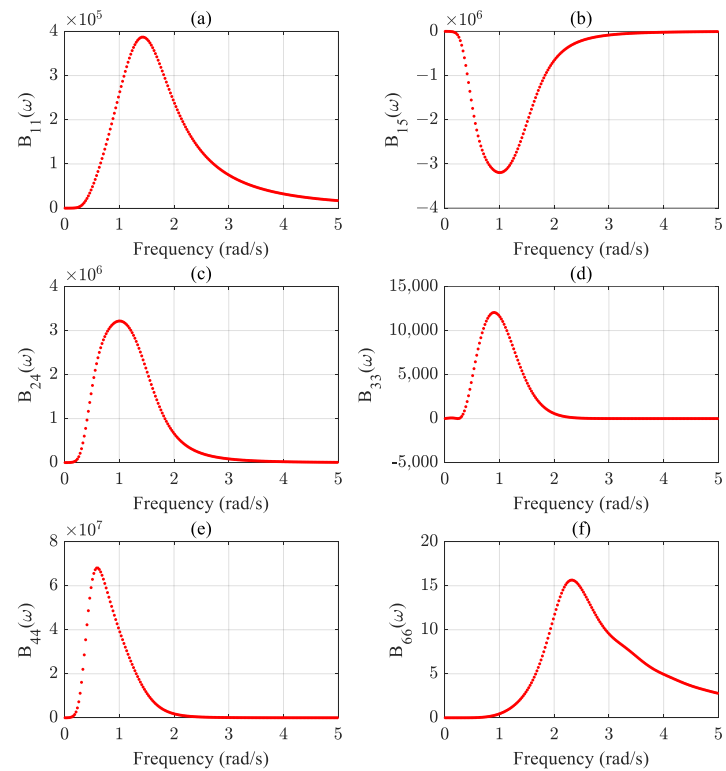


Figure 14. Potential damping for floating offshore wind turbine: (a) $B_{11}(\omega)$; (b) $B_{15}(\omega)$; (c) $B_{24}(\omega)$; (d) $B_{33}(\omega)$; (e) $B_{44}(\omega)$; and (f) $B_{66}(\omega)$.

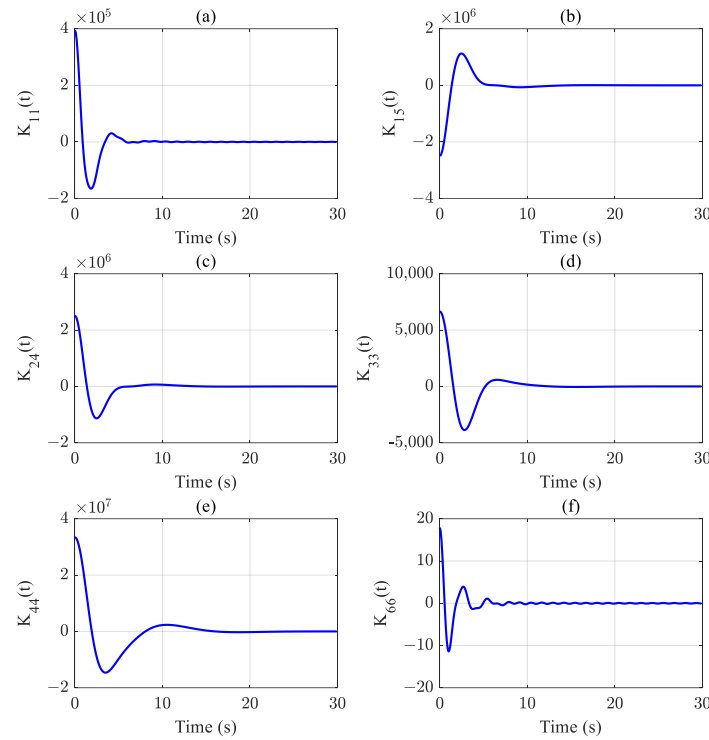


Figure 15. Time history of retardation function: (a) $K_{11}(t)$; (b) $K_{15}(t)$; (c) $K_{24}(t)$; (d) $K_{33}(t)$; (e) $K_{44}(t)$; and (f) $K_{66}(t)$.

Apart from added mass and potential damping, additional damping is another crucial hydrodynamic parameter that describes the fluid’s viscous effects. This damping is typically determined through a decay test using CFD simulations or physical model experiment. For this example, the linear additional damping values are adopted from Jonkman’s method and can be expressed as follows [36]:

$$\mathbf{B} = \begin{bmatrix} 100,000 & 0 & 0 & 0 & 0 & 0 \\ 0 & 100,000 & 0 & 0 & 0 & 0 \\ 0 & 0 & 130,000 & 0 & 0 & 0 \\ 0 & 0 & 0 & 0 & 0 & 0 \\ 0 & 0 & 0 & 0 & 0 & 0 \\ 0 & 0 & 0 & 0 & 0 & 13,000,000 \end{bmatrix} \tag{59}$$

Based on the hydrostatic and hydrodynamic parameters, the spar-type floating offshore wind turbine’s motion response will be analyzed through the application of the proposed algorithm. The effectiveness of the proposed method will be thoroughly evaluated through this application, assessing its accuracy and performance in predicting the motion response under various conditions.

3.2.2. Transfer Function Coefficients Estimation of Floating Offshore Wind Turbine

The initial step to analyze the motion response of the spar-type floating offshore wind turbine involves estimating the transfer functions in Equations (14)–(16). By substituting the parameters including hydrostatic and hydrodynamic to Equations (30)–(32), the discrete transfer functions are obtained and decoupled. Based on the discrete decoupled values and the corresponding frequency, the coefficients of the transfer functions expressed by rational fraction can be estimated by applying Equations (5)–(8). To assess the accuracy of the estimated coefficients, the comparisons of the transfer functions are plotted in Figures 16–18.

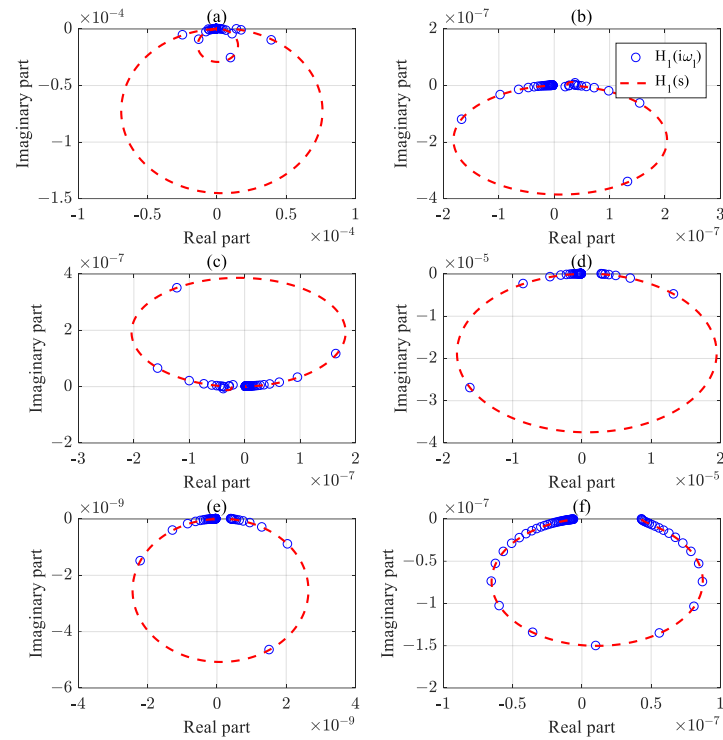


Figure 16. Initial and estimated transfer function comparison of $H_1(s)$: (a) $H_{1,11}(s)$; (b) $H_{1,15}(s)$; (c) $H_{1,24}(s)$; (d) $H_{1,33}(s)$; (e) $H_{1,44}(s)$; and (f) $H_{1,66}(s)$.

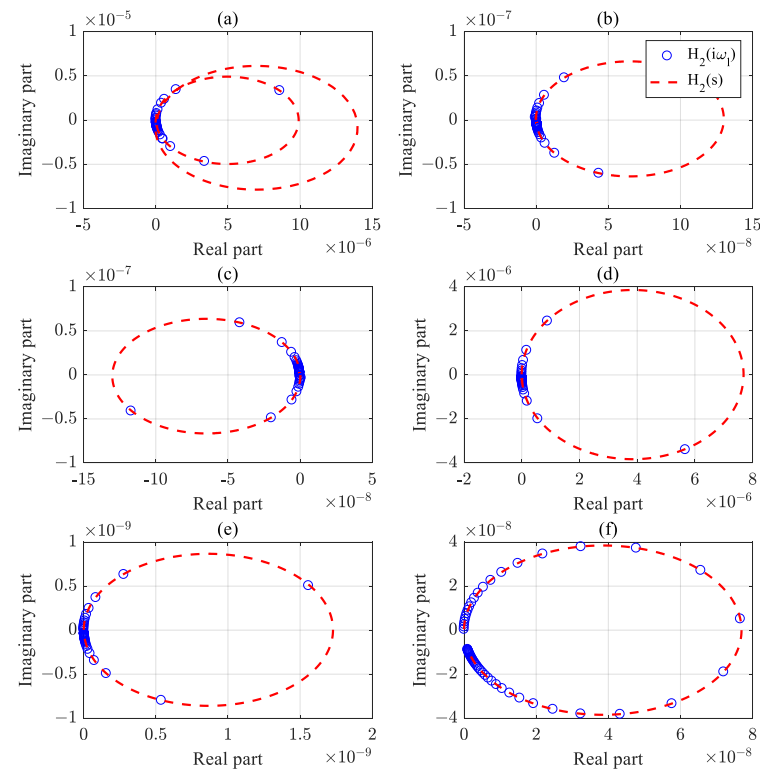


Figure 17. Initial and estimated transfer function comparison of $H_2(s)$: (a) $H_{2,11}(s)$; (b) $H_{2,15}(s)$; (c) $H_{2,24}(s)$; (d) $H_{2,33}(s)$; (e) $H_{2,44}(s)$; and (f) $H_{2,66}(s)$.

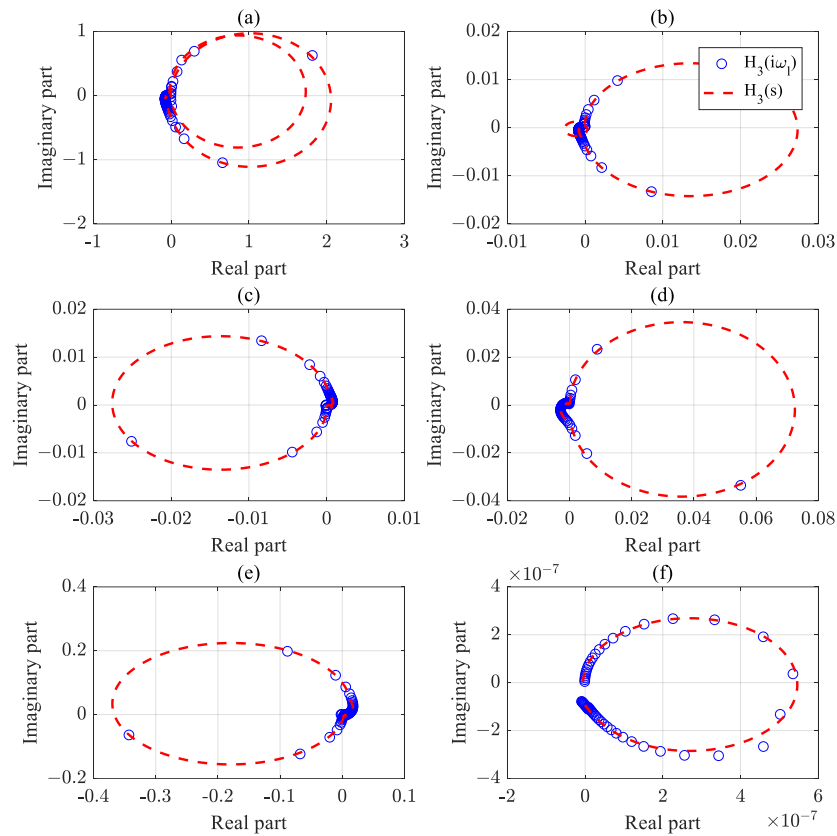


Figure 18. Initial and estimated transfer function comparison of $H_3(s)$: (a) $H_{3,11}(s)$; (b) $H_{3,15}(s)$; (c) $H_{3,24}(s)$; (d) $H_{3,33}(s)$; (e) $H_{3,44}(s)$; and (f) $H_{3,66}(s)$.

The transfer functions are complex, encompassing both real and imaginary parts. To evaluate their accuracy, the comparisons of the estimated rational fractions and the initial discrete transfer functions are plotted on the complex plane. In Figures 16–18, it can be observed that the points of the transfer function almost all lie on the curves reflecting the estimated transfer function expressions. The alignment indicates that the estimated rational fractions effectively represent the discrete transfer functions for calculating the motion response of the floating offshore wind turbine. However, it is worth noting that the estimated transfer function for $H_{3,66}(s)$ (shown in Figure 18f) does not match well with the corresponding discrete values. The transfer function $H_{3,66}(s)$ is significantly smaller than values at other positions, which suggests that the discrepancy may be due to calculation errors associated with very small values. Despite this, the discrepancy in $H_{3,66}(s)$ is five orders magnitude smaller compared to other values, indicating that the overall impact on the motion response analysis can be considered negligible.

After obtaining the expression for the transfer functions, the corresponding impulse response functions can be calculated through Equations (46)–(48). These impulse response functions are essential for calculating the motion response due to initial conditions. The impulse response functions are constructed using the poles and residues calculated via Equations (36), (44), and (45), and plotted in Figures 19–21. The figures illustrate that among the different response components, the impulse response functions for surge–surge exhibit the longest decay period. This extended decay period implies that surge–surge has the most prolonged and significant influence on the motion response caused by the initial conditions.

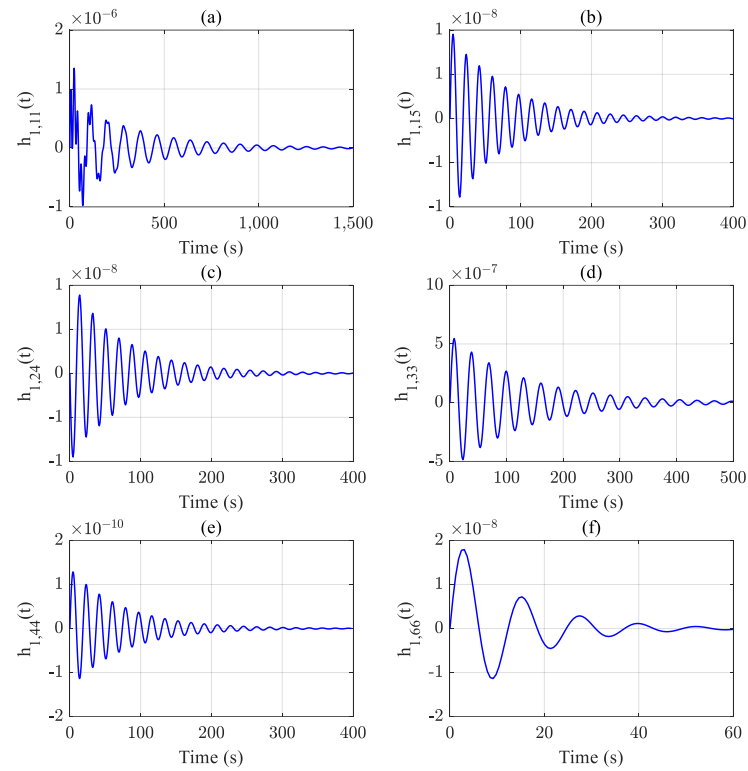


Figure 19. Impulse response function of $h_1(s)$: (a) $h_{1,11}(t)$; (b) $h_{1,15}(t)$; (c) $h_{1,24}(t)$; (d) $h_{1,33}(t)$; (e) $h_{1,44}(t)$; and (f) $h_{1,66}(t)$.

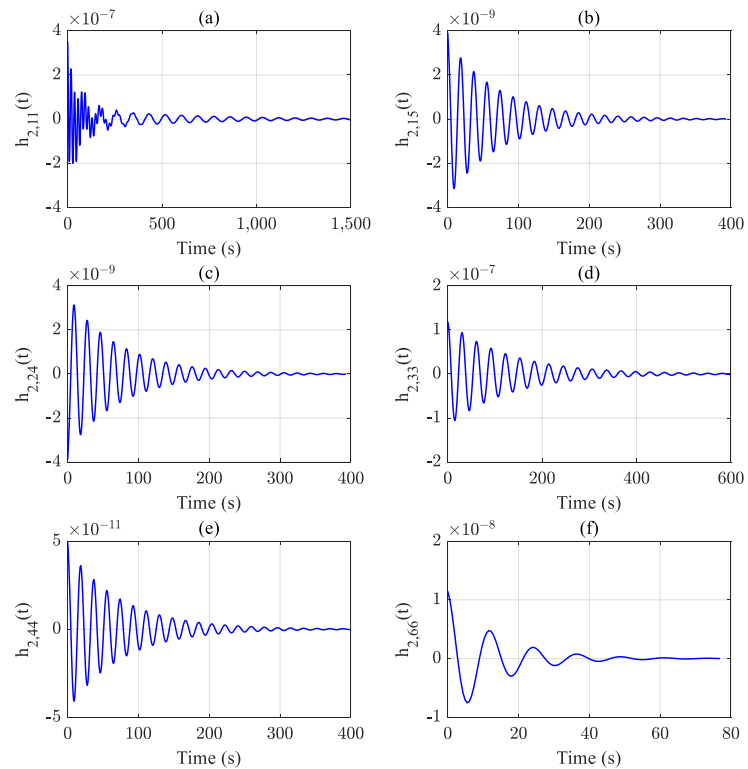


Figure 20. Impulse response function of $h_2(s)$: (a) $h_{2,11}(t)$; (b) $h_{2,15}(t)$; (c) $h_{2,24}(t)$; (d) $h_{2,33}(t)$; (e) $h_{2,44}(t)$; and (f) $h_{2,66}(t)$.

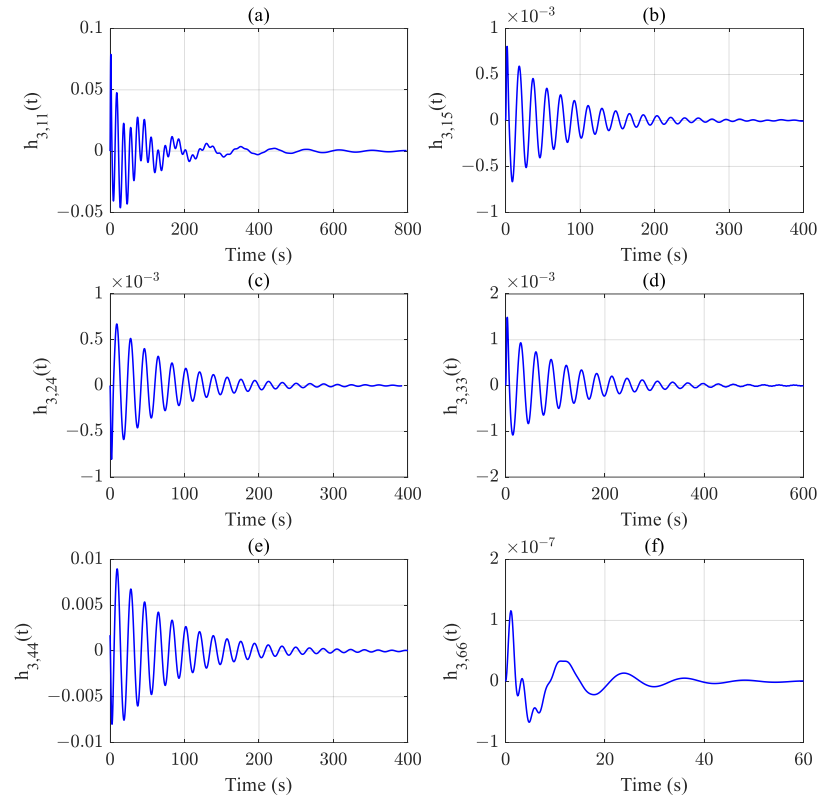


Figure 21. Impulse response function of $h_3(s)$: (a) $h_{3,11}(t)$; (b) $h_{3,15}(t)$; (c) $h_{3,24}(t)$; (d) $h_{3,33}(t)$; (e) $h_{3,44}(t)$; and (f) $h_{3,66}(t)$.

3.2.3. Transient Response Calculation of Floating Offshore Wind Turbine

This section applies the proposed method to evaluate the motion response of the spar-type floating offshore wind turbine resulting from the initial conditions. To ensure the generality of the analysis, the initial conditions are generated using random numbers, which are plotted in Figure 22.

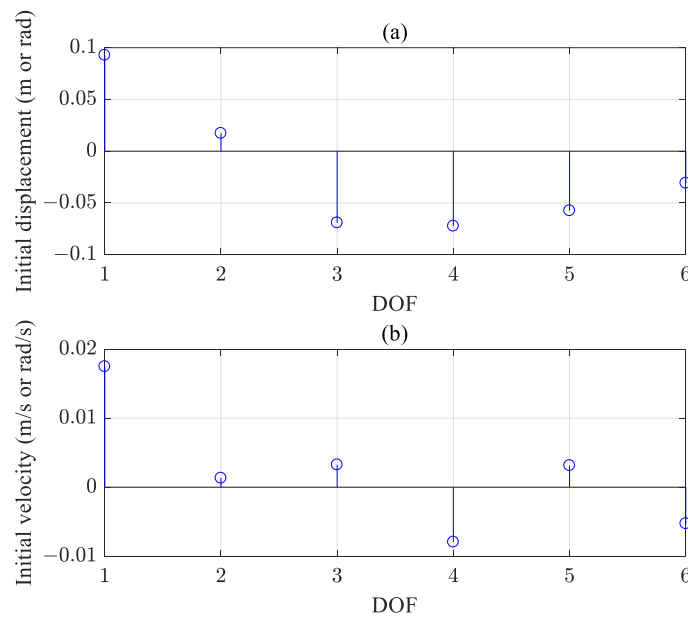


Figure 22. Initial conditions of floating offshore wind turbine: (a) displacement; and (b) velocity.

Substituting the initial conditions into Equation (33), the motions response due to the initial conditions is obtained through the superposition of impulse response functions. For comparative analysis, the Newmark- β method is applied to determine the motion response as well. The results obtained from the two methods are presented in Figure 23, which show that the motion responses calculated by the proposed method closely match those obtained using the Newmark- β method. Notably, only minor discrepancies are observed in the surge degree of freedom. The energy attenuation in the surge degree of freedom is relatively slow. With the integration time increasing, the presence of the convolution term causes the numerical damping factor of the Newmark- β method to become more pronounced, which is the primary factor contributing to the discrepancies.

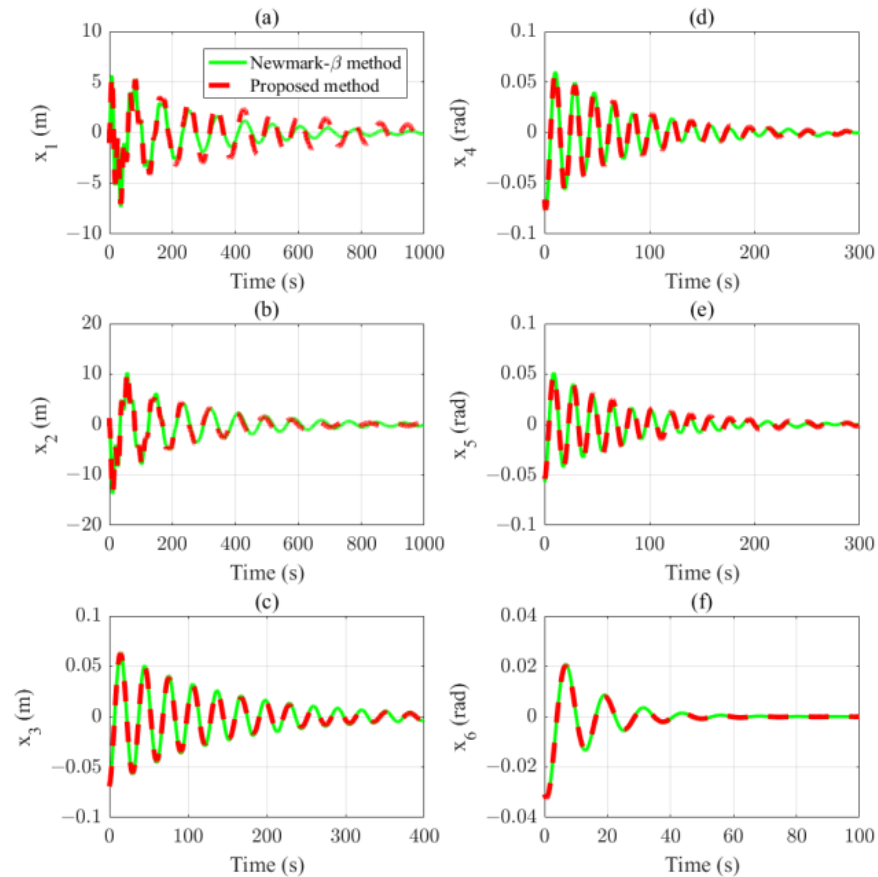


Figure 23. Comparison of motion response due to initial conditions using Newmark- β and proposed method: (a) $x_1(t)$; (b) $x_2(t)$; (c) $x_3(t)$; (d) $x_4(t)$; (e) $x_5(t)$; and (f) $x_6(t)$.

3.2.4. Motion Response Prediction of Floating Offshore Wind Turbine

The previous analysis confirms that the proposed algorithm accurately calculates the motion response of the floating offshore wind turbine due to initial conditions. This section is dedicated to assessing the performance of the proposed method in calculating motion responses triggered by wave forces. With the incident wave direction set to 0 degrees, the surge, heave, and pitch degree of freedom experience wave forces. The hydrodynamic wave force per unit amplitude is applied to determine the wave force acting on the floating foundation. The resulting wave forces are illustrated in Figure 24.

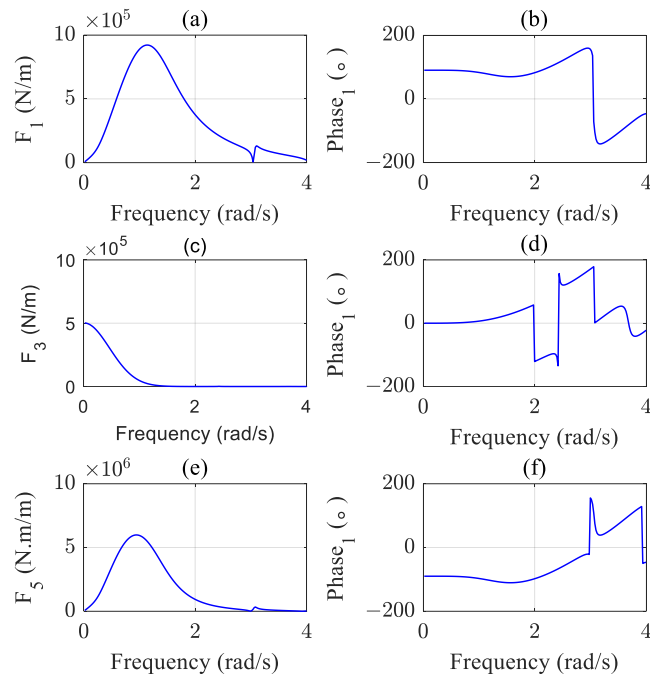


Figure 24. Hydrodynamic wave force per unit amplitude: (a) amplitude of surge; (b) phase of surge; (c) amplitude of heave; (d) phase of heave; (e) amplitude of pitch; and (f) phase of pitch.

The wave forces applied to the floating offshore wind turbine are determined by the previously hydrodynamic wave force per unit amplitude, considering both regular and irregular wave scenarios. In the case of regular wave, the wave height is set to 5 m, and the wave period is 12 s. The Jonswap wave spectrum, featuring a significant wave height of 3.5 m and a period of 10 s, is employed for the regular wave scenario.

In the case of regular waves, the hydrodynamic wave force per unit amplitude is referenced from Figure 24 according to the wave period. The amplitude of the wave force is calculated by multiplying the wave height by the hydrodynamic wave force per unit amplitude, while the phase of the wave force is taken from the phase of the hydrodynamic wave force per unit amplitude. The resulting wave force for the regular wave is plotted in Figure 25.

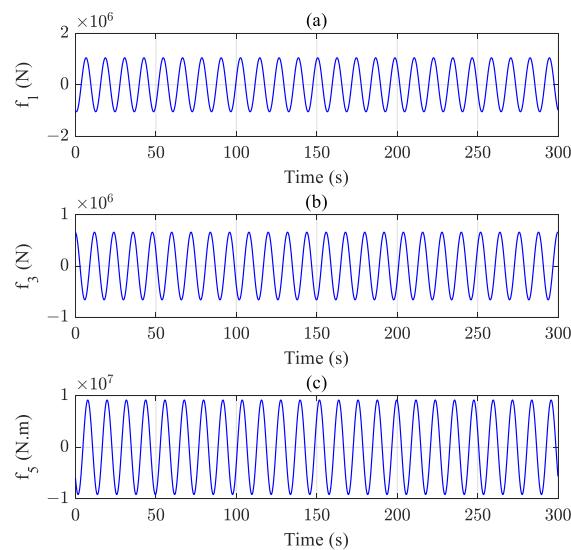


Figure 25. Regular wave force: (a) surge; (b) heave; and (c) pitch.

According to Equation (42), the state-space model for transfer function $H_s(s)$ is constructed based on the previously estimated poles and residues. In this model, the wave forces are the input of the state-space model system, and the motion responses due to the wave forces are the outputs. By employing this state-space model, the motion response can be calculated with relative ease. The outcomes are compared with the results from the Newmark- β method. The comparison figures are shown in Figure 26, demonstrating a good match between the two methods, indicating the effectiveness of the proposed algorithm in accurately computing the motion response of the floating offshore wind turbine under wave forces.

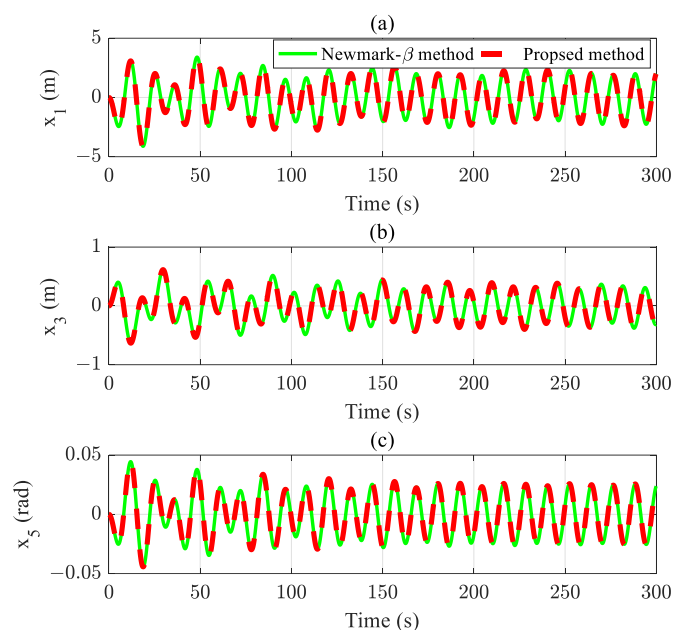


Figure 26. Calculated motion response excited by regular wave: (a) $x_1(t)$; (b) $x_3(t)$; and (c) $x_5(t)$.

To conduct a more detailed examination of the proposed method, the floating offshore wind turbine is subjected to irregular wave conditions, with the significant wave height of 3.5 m and the peak period of 10 s. The corresponding Jonswap spectrum is used to simulate the irregular wave, as plotted in Figure 27.

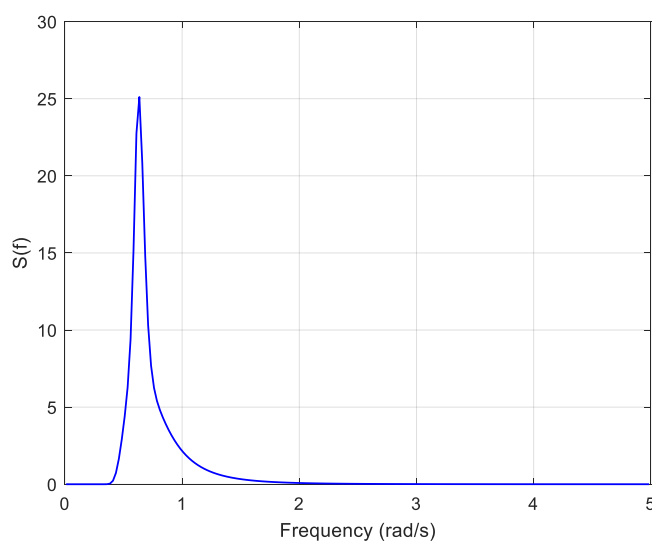


Figure 27. Jonswap spectrum to simulate irregular waves.

The Jonswap spectrum allows for the determination of the wave height of each component of the irregular wave. The amplitudes of wave forces corresponding to each wave component are determined by the hydrodynamic wave force per unit amplitude, and the corresponding phases are generated using a series of random seeds. The wave force exerted by the irregular wave on the floating offshore wind turbine is calculated by superimposing each component, as plotted in Figure 28.

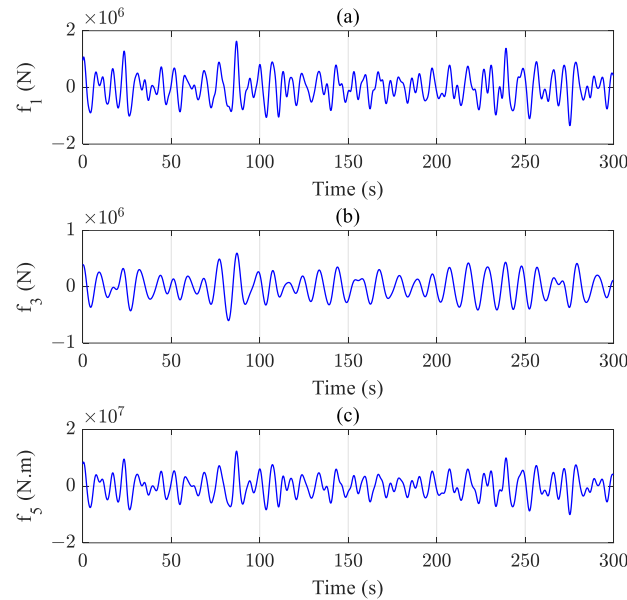


Figure 28. Irregular wave force: (a) surge; (b) heave; and (c) pitch.

The irregular wave force is also substituted into the calculated state-space model, and the calculation of the motion response of the floating offshore wind turbine due to the irregular wave force is performed in the same way. The result comparison between the proposed and Newmark- β method is shown as Figure 29, demonstrating good agreement between the two methods.

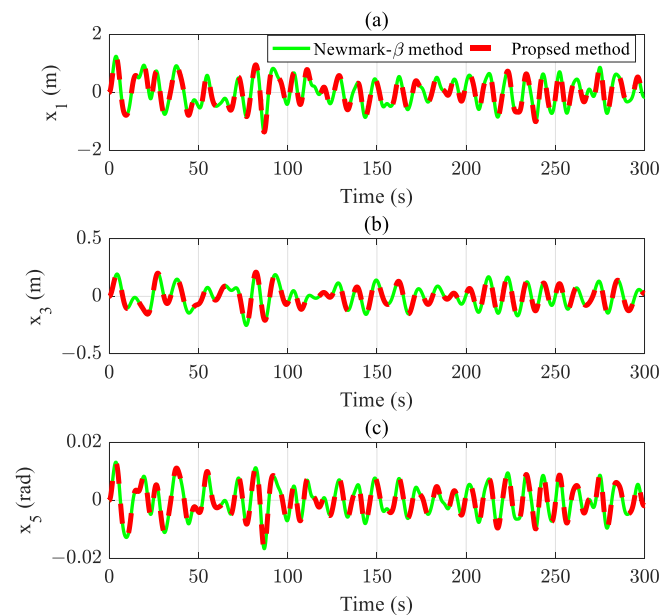


Figure 29. Calculated motion response excited by irregular wave: (a) $x_1(t)$; (b) $x_3(t)$; and (c) $x_5(t)$.

3.2.5. Computational Efficiency Analysis of Proposed Method

The conventional time-domain technique involves solving the Cummins equation via incremental integration, which can result in inefficient computations due to the convolution integrals involved. In contrast, the proposed algorithm rephrases the problem of motion prediction as a system output acquisition task, thereby eliminating the need for convolution integrals and potentially enhancing computational efficiency.

To evaluate the computational efficiency of the proposed algorithm, simulations were conducted over various durations—100 s, 200 s, 300 s, 400 s, 500 s, 600 s, 700 s, 800 s, 900 s, and 1000 s—using irregular wave conditions. Both the proposed and Newmark- β method were employed to estimate the motions responses of the spar-type floating offshore wind turbine. The CPU times for the two methods were documented while executing MATLAB code on a system featuring an Intel Core i7-8700 CPU and 16 GB of RAM.

The results, as shown in Figure 30, indicate that the proposed method significantly outperforms the traditional time-domain method in terms of computational efficiency. This improvement is especially notable for longer simulation durations, demonstrating that the proposed algorithm offers a more efficient approach for motion response analysis in floating offshore wind turbines.

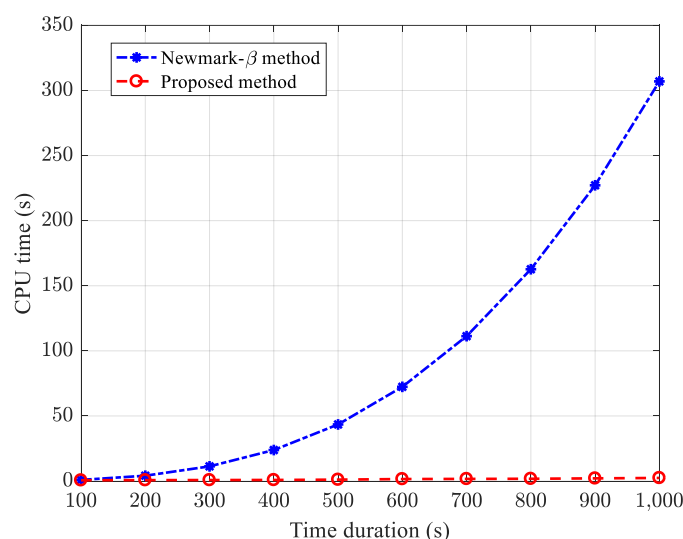


Figure 30. Time consumption of proposed and Newmark- β .

4. Conclusions

This paper presents an innovative approach for predicting the motion response of floating offshore wind turbines, utilizing transfer functions and state-space models to address the computational inefficiencies often encountered with traditional time-domain methods. The proposed transforms the response calculation problem into a system output problem, bypassing convolution integrals and thereby enhancing computational efficiency. The method begins with the estimation of transfer functions from hydrostatic and hydrodynamic parameters, essential for accurate motion response prediction. These transfer functions are then used to construct corresponding state-space models. Motion responses due to initial conditions and wave forces are calculated using these models and the poles and residues.

Validation of the proposed method was performed initially on an SDOF system. Comparisons with the Newmark- β method demonstrated that the proposed approach matches the accuracy of the traditional method. The method's effectiveness was further evaluated using an MDOF system represented by a spar-type floating offshore wind turbine. Simulations involving regular and irregular waves demonstrated the method's

robustness. Regular wave simulations used a wave height of 5 m and a period of 12 s, while irregular wave simulations were applied to the Jonswap spectrum with a significant wave height of 3.5 m and a peak period of 10 s. The calculated wave forces were input into the state-space model to determine the motion response. Comparison of results from the proposed and Newmark- β method showed high accuracy and agreement. Moreover, the computational efficiency of the proposed algorithm was rigorously tested across various simulation durations, consistently showing significant reductions in computation times compared to the traditional method, particularly in long-duration simulations.

In conclusion, the proposed method offers a robust and efficient alternative for predicting the motion response of floating offshore wind turbines. By avoiding convolution integrals and employing state-space models, it achieves high accuracy and improved computational efficiency. This method is poised to become a valuable tool in the design and analysis of offshore wind energy systems, offering substantial benefits in terms of both precision and speed. The convolution term in Cummins equation is the main factor limiting the computational efficiency and accuracy of the motion response of floating structures. For multi-body systems, as the degrees of freedom increase, the number of convolution terms that need to be calculated also increases rapidly. Therefore, the proposed method provides an alternative approach for motion response analysis of multi-body renewable energy devices.

Author Contributions: Software, J.X. and C.L.; investigation, W.J. and F.L.; funding acquisition, S.L.; writing—original draft preparation, H.L.; writing—review and editing, H.W. All authors have read and agreed to the published version of the manuscript.

Funding: This research was funded by the National Natural Science Foundation of China (grant no. 52371296, 52071145), Key Technology Research Task of Floating Offshore Combined Wind and Wave Power Generation (grant no. DTGD-2023-10174), New Energy Joint Laboratory of China Southern Power Grid Corporation (grant no. GDXNY2022KF03), and the “CUG Scholar” Scientific Research Funds at China University of Geosciences (Wuhan) (grant no. 2022151).

Institutional Review Board Statement: Not applicable.

Informed Consent Statement: Not applicable.

Data Availability Statement: The data used and analyzed during the current study will be available from the corresponding author upon reasonable request after publication of this article.

Conflicts of Interest: Authors Jie Xu and Changjie Li were employed by the company Guangdong Datang International Chaozhou Power Generation Co., Ltd. Authors Wei Jiang and Fei Lin were employed by the company China Datang Co., Ltd. Guangdong Branch. Author Shi Liu was employed by the company China Southern Power Grid Electric Power Technology Co., Ltd. The remaining authors declare that the research was conducted in the absence of any commercial or financial relationships that could be construed as a potential conflict of interest.

References

1. Oh, K.Y.; Nam, W.; Ryu, M.S.; Kim, J.Y.; Epureanu, B.I. A review of foundations of offshore wind energy converters: Current status and future perspectives. *Renew. Sustain. Energy Rev.* **2018**, *88*, 16–36. [[CrossRef](#)]
2. Zhang, W.Z.; Calderon-sanchez, J.; Duque, D.; Souto-Iglesias, A. Computational Fluid Dynamics (CFD) applications in Floating Offshore Wind Turbine (FOWT) dynamics: A review. *Appl. Ocean Res.* **2024**, *150*, 104075. [[CrossRef](#)]
3. Yang, L.; Li, B.B.; Dong, Y.H.; Hu, Z.Z.; Zhang, K.; Li, S.W. Large-amplitude rotation of floating offshore wind turbines: A comprehensive review of causes, consequences, and solutions. *Renew. Sustain. Energy Rev.* **2025**, *211*, 115295. [[CrossRef](#)]
4. Faraggiana, E.; Giorgi, G.; Sirigu, M.; Ghigo, A.; Bracco, G.; Mattiazzo, G. A review of numerical modelling and optimization of the floating support structure for offshore wind turbines. *J. Ocean Eng. Mar. Energy* **2022**, *8*, 433–456. [[CrossRef](#)]

5. Matha, D.; Schlipf, M.; Cordle, A.; Pereira, R.; Jonkman, J. Challenges in simulation of aerodynamics, hydrodynamics, and mooring-line dynamics of floating offshore wind turbines. In Proceedings of the 21st Offshore and polar Engineering Conference, Maui, HI, USA, 19–24 June 2011.
6. Partovi-Mehr, N.; Branlard, E.; Song, M.; Moaveni, B.; Hines, E.M.; Robertson, A. Sensitivity Analysis of Modal Parameters of a Jacket Offshore Wind Turbine to Operational Conditions. *J. Mar. Sci. Eng.* **2023**, *11*, 1524. [[CrossRef](#)]
7. Zahle, F.; Sørensen, N.N.; Johansen, J. Wind turbine rotor-tower interaction using an incompressible overset grid method. *Wind Energy* **2009**, *12*, 594–619. [[CrossRef](#)]
8. Taghipour, R.; Perez, T.; Moan, P. Hybrid frequency-time domain models for dynamic response analysis of marine structures. *Ocean Eng.* **2008**, *35*, 685–705. [[CrossRef](#)]
9. Li, Y.W.; Paik, K.J.; Xing, T.; Carrica, P.M. Dynamic overset CFD simulations of wind turbine aerodynamics. *Renew. Energy* **2012**, *37*, 285–298. [[CrossRef](#)]
10. Cai, Y.F.; Li, X.; Leng, S.D.; Zhao, H.S.; Zhou, Y. Effect of combined surge and pitch motion on the aerodynamic performance of floating offshore wind turbine. *Ocean Eng.* **2024**, *306*, 118061. [[CrossRef](#)]
11. Yang, H.S.; Tongphong, W.; Ali, A.; Lee, Y.H. Comparison of different fidelity hydrodynamic-aerodynamic coupled simulation code on the 10 MW semi-submersible type floating offshore wind turbine. *Ocean Eng.* **2023**, *281*, 118061. [[CrossRef](#)]
12. Tran, T.T.; Kim, D. A CFD study of coupled aerodynamic-hydrodynamic loads on a semisubmersible floating offshore wind turbine. *Wind Energy* **2018**, *21*, 70–85. [[CrossRef](#)]
13. Zhou, Y.; Xiao, Q.; Peyrard, C.; Pan, G. Assessing focused wave applicability on a coupled aero-hydro-mooring FOWT system using CFD approach. *Ocean Eng.* **2021**, *240*, 109987. [[CrossRef](#)]
14. Liu, Y.C.; Xiao, Q.; Incecik, A.; Peyrard, C.; Wan, D. Establishing a fully coupled CFD analysis tool for floating offshore wind turbines. *Renew. Energy* **2017**, *112*, 280–301. [[CrossRef](#)]
15. Rodrigues, R.V.; Lengsfeld, C. Development of a computational system to improve wind farm layout, part ii: Wind turbine wakes interaction. *Energies* **2019**, *12*, 1328. [[CrossRef](#)]
16. Newman, J. *Marine Hydrodynamics*; MIT Press: Cambridge, MA, USA, 1977.
17. Faltinsen, O. *Hydrodynamic of High-Speed Marine Vehicles*; Cambridge University Press: Cambridge, UK, 2005.
18. Ramachandran, G.K.V.; Robertson, A.; Jonkman, J.M.; Masciola, M.D. *Investigation of Response Amplitude Operators for Floating Offshore Wind Turbines*; National Renewable Energy Lab. (NREL): Golden, CO, USA, 2013.
19. Lu, H.C.; Fan, T.H.; Chen, C.H.; Sun, Z.Z. Pole-residue method for dynamic response analysis of floating structures depending on decoupled Cummins equation. *Ocean Eng.* **2022**, *246*, 110414. [[CrossRef](#)]
20. Cummins, W.E. The impulse response function and ship motions. *Schiffstechnik* **1962**, *9*, 101–109.
21. Jorge, D.E.; Laura, B.; Mario, S. A semi-analytical computation of the Kelvin kernel for potential flows with a free surface. *Comput. Appl. Math.* **2011**, *30*, 267–287.
22. Clement, A.H. A second order ordinary differential equation for the frequency domain Green function. In Proceedings of the 28th International Workshop on Water Waves and Floating Bodies, L'Isle-sur-la-Sorgue, France, 7–10 April 2013.
23. Xie, C.M.; Chen, X.B.; Alain, H.C.; Aurelien, B. A new ordinary differential equation for the evaluation of the frequency-domain Green function. *Appl. Ocean Res.* **2019**, *86*, 239–245. [[CrossRef](#)]
24. Ogilvie, T. Recent progress towards the understanding and prediction of ship motions. In Proceedings of the 5th Symposium on Naval Hydrodynamics, Bergen, Norway, 10–12 September 1964.
25. Wang, Y.G. Robust frequency-domain identification of parametric radiation force models for a floating wind turbine. *Ocean Eng.* **2015**, *109*, 580–594. [[CrossRef](#)]
26. Barrera, C.; Battistella, T.; Guanache, R.; Losada, I. Mooring system fatigue analysis of a floating offshore wind turbine. *Ocean Eng.* **2020**, *195*, 106670. [[CrossRef](#)]
27. Chen, C.H.; Ma, Y.; Fan, T.F. Review of model experimental methods focusing on aerodynamic simulation of floating offshore wind turbines. *Ocean Eng.* **2022**, *157*, 112036. [[CrossRef](#)]
28. Kashiwagi, M. Transient response of a VLFS during landing and take-off of an airplane. *J. Mar. Sci. Technol.* **2004**, *9*, 14–23. [[CrossRef](#)]
29. Liu, F.S.; Chen, J.F.; Qin, H.D. Frequency response estimation of floating structures by representation of retardation functions with complex exponentials. *Mar. Struct.* **2017**, *54*, 144–166. [[CrossRef](#)]
30. Perez, T.; Fossen, T.I. Practical aspects of frequency-domain identification of dynamic models of marine structures from hydrodynamic data. *Ocean Eng.* **2011**, *38*, 426–435. [[CrossRef](#)]
31. Lu, H.C.; Chang, S.; Chen, C.H.; Fan, T.H.; Chen, J.F. Replacement of force-to-motion relationship with state-space model for dynamic response analysis of floating offshore structures. *Appl. Ocean Res.* **2022**, *119*, 102977. [[CrossRef](#)]
32. Liu, B.; Yu, J. Dynamic Response and Mooring Fracture Performance Analysis of a Semi-Submersible Floating Offshore Wind Turbine Under Freak Waves. *J. Mar. Sci. Eng.* **2024**, *12*, 1414. [[CrossRef](#)]

33. Lu, H.C.; Tian, Z.; Zhou, L.; Liu, F.S. An improved time-domain response estimation method for floating structures based on rapid solution of a state-space model. *Ocean Eng.* **2019**, *173*, 628–642. [[CrossRef](#)]
34. Shabara, M.A.; Abdelkhalik, O. Dynamic modeling of the motions of variable-shape wave energy converters. *Renew. Sust. Energ. Rev.* **2023**, *173*, 113070. [[CrossRef](#)]
35. Lu, H.C.; Fan, T.H.; Zhou, L.; Chen, C.H.; Yu, G.M.; Li, X.C.; Hou, F.L. A rapid response calculation method for symmetrical floating structures based on state-space model solving in hybrid time-Laplace domain. *Ocean Eng.* **2020**, *203*, 107227. [[CrossRef](#)]
36. Jonkman, J. *Definition of the Floating System for Phase IV of OC3 (No. NREL/TP-500-47535)*; National Renewable Energy Lab. (NREL): Golden, CO, USA, 2010.

Disclaimer/Publisher’s Note: The statements, opinions and data contained in all publications are solely those of the individual author(s) and contributor(s) and not of MDPI and/or the editor(s). MDPI and/or the editor(s) disclaim responsibility for any injury to people or property resulting from any ideas, methods, instructions or products referred to in the content.